EUROPEAN CENTRE FOR MEDIUM RANGE WEATHER

FORECASTS

TECHNICAL REPORT
****

NO. 5
*****

JULY

1977
****

****

**

A Study of some Parameterisations of Sub-Grid Processes in a Baroclinic Wave in a Two-Dimensional Model

By

A. Hollingsworth

EUROPEAN CENTRE FOR MEDIUM RANGE WEATHER FORECASTS

Fitzwilliam House
Skimped Hill
Bracknell, Berkshire
United Kingdom

CONTENTS PAGE NUMBER

A B S T R A C T

In this study we use a two-dimensional slab version of the ECMWF model to examine the effects of sub-grid scale parameterisations on an idealised baroclinic wave. The parameterisations studied were those of the GFDL model (Manabe et al 1965) apart from Radiation, the Convection Scheme of Kuo (1974), the Multipoint Filter of Shapiro (1970) and the Dry Convection Parameterisation of Corby et al(1972). The main finding is that the Kuo convection scheme has a more gradual effect on the flow than the Manabe scheme. The Manabe scheme can produce large changes in the vorticity field in a two-hour period even in mid latitudes.

The synoptic evolution using the schemes is rather different in some circumstances. In one set of experiments we found what appeared to be a secondary cold-front using the Manabe scheme, but not with the Kuo scheme.

1. Introduction

The problem of parameterisation of the sub-grid scale processes has a number of aspects. In the first place there is the observational effort to relate the sub-grid scale turbulent transports to the large scale field. Secondly there is the question of the interaction between the dynamics and the parameterisation in the course of an integration. The turbulent fluxes due to a parameterisation may be reasonably accurate at most grid points in a given time step. If, however, the cumulative effect of the formulation being used produces computational problems or unrealistic features we may wish to modify the formulation to reduce such problems.

The study of this latter question is usually done with three-dimensional models which are, of course, expensive to integrate. Part of the motivation for this study was to see if a less expensive two-dimensional model could be useful in this regard. The results discussed below indicate that two commonly used convective schemes have markedly different effects on the development of a front.

It is expected that research workers in ECMWF's member countries will want to use the ECMWF model for experimental work in the field of parameterisation. The two-dimensional model provides a convenient means for these workers to develop and test their codes in their home environment. The codes can then be readily implemented in the ECMWF three-dimensional model for experiments at ECMWF.

This report describes the use of the model to study the effect of a number of physical parameterisations on the growth of a large scale baroclinic wave. In Sections 2 and 3 we describe the finite difference scheme and grid, and the specification of initial and boundary conditions. In Section 4 we describe the evolution of the growing wave in the presence of a weak internal smoothing. In Section 5 we summarise the main features of the parameterisations used. In Section 6 we describe the evolution of the baroclinic wave in the presence of parameterisations of the surface exchanges, the planetary boundary layer and dry convection. In Section 7 we discuss the effect on the wave of including, in addition, the effect of moist convection. We used the schemes proposed by KUO (1974) and MANABE (1965). We found that there were important differences between these schemes in their effect on the dynamical fields in the early stages of the growth of the wave. In Section 8 we discuss the later stages of growth and show that these dynamical differences persist and amplify. In one set of experiments a secondary cold front developed using the MANABE scheme but not the KUO scheme. In general the KUO scheme causes gradual changes in the flow field while the MANABE scheme produces sudden and quite sharp changes. In Section 9 we discuss the effect of internal dissipation on the computational noise in the integrations. For reasonable values of the coefficients in the linear fourth order dissipation and the non-linear SMAGORINSKY (1965) dissipation the noise levels are about the same.

2. Finite Difference Model

The model used is a version of the three-dimensional ECMWF model (BURRIDGE 1977). The finite difference scheme is written in advective form on a staggered latitude-longitude grid. The scheme is energy conserving and in addition conserves the mean of p^*Z^2 for horizontal flow where p^* is surface pressure and Z is the vertical component of the absolute potential vorticity. In the vertical, σ-coordinates are used.

The model is made two-dimensional in the following manner: All geometric constants are fixed for a given latitude (in the present case 40^o). The meridional gradients of u, v and p^* are set to zero, while those of T and q are specified and held constant.

The three-dimensional code is organised so that at latitude j all north south advections between j and j-1 are known. Then Z_{j+1} and the advections between j and j+1 are calculated. Finally the tendency can be calculated by combining the advections and the linear terms. In the two-dimensional model we use the same code and make three passes through it skipping over selected portions on each pass. On the first pass we calculate Z_{j-1} (and so Z_j, Z_{j+1}). On the second pass we calculate the advections between j-1 and j. On the third pass we calculate the advections between j+1 and j, and finally the tendencies.

The baroclinic wave studied had wave length equal to that of wave number 6 at 40^oN viz. 5,100 km. This is reasonably close to the wave-length of maximum instability for the zonal wind profile used. We used 48 grid points in the east-west direction giving a resolution of 106 km, which is close to what we hope will be possible in the ECMWF operational model.

The vertical grid was defined following SMAGORINSKY et al (1965) viz.

$$\sigma_k = s_k^2 (3-2s_k),\ s_k = (2k-1)/18,\ k = 1,2 \text{ --- } 9,$$

giving a nine level model. This was done to facilitate the introduction of the radiation scheme of the GFDL model in later experiments.

The time scheme was an explicit leap frog scheme with a time step of 90 secs.

3. Initial Conditions and Resolution

The initial conditions for most of the runs described below were derived in the following way :
The north south gradient of temperature at each level,

$$\left(\frac{\partial \bar{T}}{\partial y}\right)_k$$

was calculated from the zonal wind profile shown in Fig. 1.

The temperature gradient was derived by specifying $\bar{u}$ analytically to increase linearly from 0 to 25 m/sec in σ=1, 0.25 and decrease linearly to 0 at σ = 0. We differentiate this $\bar{u}$ with the model's hydrostatic equation to calculate $\frac{\partial \bar{T}}{\partial y}$.

This field had some small two-grid wave features because of the form of the hydrostatic equation (HOLLINGSWORTH 1976).

$\frac{\partial \bar{T}}{\partial y}$ was therefore smoothed slightly to remove this feature and the hydrostatic equation was integrated to calculate the final $\bar{u}$ shown.

There is a jet maximum of 23 m/sec near the tropopause. The zonally averaged temperature initially, T_o, was that of the standard atmosphere. Table 1 lists the values of $\bar{u}$, T_o, $\frac{\partial \bar{T}}{\partial y}$.

TABLE 1: The values of , T_o, $\frac{\partial T}{\partial y}$ and $\bar{u}$ at the model levels.

	σ	T_o ^oK	$\frac{\partial \bar{T}}{\partial y}$ $^oK/m$	$\bar{u}$ m/s
k = 1	.009	216	-2.68E-7	.25
2	.074	216	-3.36E-6	6.99
3	.188	216	-7.72E-6	19.36
4	.336	233	4.98E-6	23.33
5	.500	251.1	6.71E-6	17.58
6	.664	265.5	9.59E-6	11.93
7	.812	275	1.12E-5	6.77
8	.926	283	1.31E-5	2.84
9	.991	287	1.39E-5	.6

To T_o was added a perturbation temperature of the form shown in Figure 2b which has no phase variation with height. This was balanced by a north south velocity field of the form shown in Figure 2a.

If the model is integrated forward from these initial conditions the perturbation grows and changes its form so as to have a westward phase tilt with height. For the adiabatic integration discussed below the integration was allowed to continue in this way.

To discuss the initial conditions for the diabatic integrations we must specify the mean mixing ratio - gradient. It can be specified as either a linear or a logarithmic function of latitude. A linear specification of the form

$$\left(\frac{\partial q}{\partial y}\right)_k = \left(\frac{\partial}{\partial T} q_s\right)\Bigg|_{\substack{T=T_o(k) \\ y=o \\ t=o}} \cdot \left(\frac{\partial \bar{T}}{\partial y}\right)_k = \text{constant at each level}$$

has the disadvantage that for the north-south temperature gradients used a relative humidity of 75 % at any level implied negative mixing ratios in the basic state some 600 - 800 km to the north.

A wind of 10 m/sec lasting for a day would thus produce a negative q in the model. A further disadvantage of this choice is that the relative humidity of air advected from the south becomes progressively lower. This is because the saturation vapour pressure is an exponential rather than a linear function of temperature. Even though the mixing ratio increases to the south the saturation mixing ratio increases more rapidly to the south with a consequent decrease of the relative humidity. The problem of the negative humidities in the basic state may be circumvented by requiring that the humidity cannot become negative. In effect we permit only poleward moisture advection after a certain stage. For our purposes this is not a serious restriction.

For reasons described below, in some experiments we specified the north south gradients of q logarithmically by

$$q_{j-1,k} = \alpha_k q_{j,k}$$

$$q_{j+1,k} = \frac{1}{\alpha_k} q_{j,k}$$

where

$$\alpha_k = 1 + \frac{d}{dy}\left(\ell n\ e_s\right)\Big|_{y\,=\,0,\ \tau=0}$$

We thus have

$$\left(q_{j-1,k} - q_{j,k}\right)/q_{jk} = \left(\frac{d}{dy}\ (\ell n\ e_s)\right)\ y = 0,\ t = 0$$

Now

$$\frac{d}{dy}\ \ell n\ e_s = -\frac{L}{R\bar{T}^2}\ \frac{d\bar{T}}{dy}\ ,$$

$\frac{d\bar{T}}{dy}$ is fixed and the variation of $-\frac{L}{RT^2}$ is nearly linear in T.

The changes of temperature produced in the model in the integrations for which humidity plays a role is no more than 15°K. Hence

$$\frac{L}{RT^2}$$

will vary by no more than 10 %. This has the advantage of keeping the relative humidity of the advected air nearly constant.

The initial state for the runs with convective schemes was obtained by integrating from day zero to day 1½ with the following parameterisations described in paragraph 5:

(1) Surface layer
(2) Planetary boundary layer
(3) Dry convection as an adjustment process
(4) Large scale condensation
(5) ∇^4 smoothing and time filter
(6) Linear gradient in humidity.

This yields the fields shown in Fig. (3). The westward phase tilt is well established. There has been practically no large scale condensation and the relative humidity is just approaching 100 % in the warm air. If we included the MANABE convection scheme in the run there would have been no convective rain to this point. On the other hand if we had included the KUO convective scheme there would have been enough convection to change the vertical velocity field considerably though the other fields would be relatively unchanged. It was to avoid this distortion that we took the fields as described at day 1.5 as the initial state and then changed the north-south humidity gradient at that time to a logarithmic specification if we so required.

4. Adiabatic Integration

The quasi-geostrophic theory of baroclinic instability is well known (CHARNEY (1947), EADY (1949)). The present initial flow is unstable and on linear theory we would expect unstable normal modes to grow exponentially in time, with the most unstable mode becoming dominant. The perturbations would have a sinusoidal form in the east west. Fig. 4 shows the perturbation fields of u, V, T at day 3 with a weak time filter $\nu = .02$ and horizontal smoothing $K_4 \nabla^4$; $K_4 = 7 \times 10^{15}$.

Fig. 5 shows the patterns of p at the surface, V,T at the lowest level at the day 3. The results in the later stages are very similar to those found by WILLIAMS (1967) in a very similar experiment.

There is very little growth in the eddy kinetic energy during the first two days. The initial perturbation is not a normal mode and the most unstable normal mode does not become apparent

in the fields until about day 1½. Thereafter the growth is rapid. However, the sinusoidal form is not maintained as the perturbation grows to large amplitude. The region of positive vorticity shrinks and the magnitude of the vorticity in the region increases while the reverse happens in the region of negative vorticity. This effect has been discussed by HOSKINS (1975) and HOSKINS and BRETHERTON (1972). The latter authors give a very complete analysis of the closely related experiment by WILLIAMS (1967). They show that the region of large vorticity will collapse to a discontinuity in a finite time given the infinite source of energy in the model.

According to quasi-geostrophic theory for the Eady problem, there is a phase difference of a quarter wave-length between the V and T waves. In the analysis of HOSKINS and BRETHERTON (1972) the same solution is found to apply in the transformed coordinate space.

$$(X,Z) = (x + \frac{V_g}{f}, z)$$

where x is the east west coordinate, V_g is the geostrophic V velocity and z a vertical coordinate. In their analysis the transformation back to physical space has the effect of bringing the regions of positive shear in V, T into much closer coincidence than in the quasi-geostrophic solution, so that the entire flow near the vorticity maximum bears a close resemblance to the classical model of a cold front. In our integrations this coinciding of the V and T shear maxima does not occur until the late stages of the development. By this time the shears have become so large that the model breaks down. At day 3 at the lowest layer (Fig.5) the zero perturbation isotherm still lags the zero isotach in V by about one eighth of a wave-length or 650 km, although the zones of maximum shear in V, T differ by only one grid length.
This feature is clearly related to the fact that the meridional wind near the surface is significantly larger on the warm side of the shear line. A similar feature may be seen in the BOUSSINESQ integrations of WILLIAMS (1967).

In Fig. 6 we show the fields of $p^* \dot{\sigma}$ and of q, the humidity mixing ratio, at day 3. The units for $p^*\dot{\sigma}$ are Pascals/sec. 1 Pa/sec. is 36 mb/hr. At the surface 1 Pa/sec. is 8 cm/sec. At day 2, when the wave was still in the linear regime the pattern of $p^* \dot{\sigma}$ was essentially sinusoidal in the east west coordinate. By day 3 however the non-linear frontogenesis is well advanced. The rising motion ahead of the front has been concentrated into a narrow region with $p^* \dot{\sigma}$ reaching a value of -.49 Pa/sec. (~17.5 mb/hr.). The region of descent is much broader with a maximum value near the front of .11 p/sec (~4 mb/hour).

The field of q reflects the combined effects of horizontal and vertical advection. The subsiding cold air is dry and the rising warm air is quite moist. The model therefore behaves according to expectation in this adiabatic integration. There is no generation of computational noise though the internal dissipation is modest. Fig. 7 shows longitudinal spectra of the ageostrohpic wind component u' at the levels 4,5,9 (330,500,990 mb approx.) at day 3. Wave number 12 is the 4 Δx wave and wave number 24 is

the 2 Δx wave. In Fig. 8 we see that even with the very large shears present in the model there is very little energy in wave lengths shorter than 4 Δx.

5. Parameterisation of Sub-Grid Scale Processes

The parameterisations used in these experiments are described in detail in MANABE et al GARP Report 14 (1974, p 7), KUO (1974), SHAPIRO (1971), CORBY, GARP Report 14 (1974, p 113). Here we present brief summaries of the main features of the parameterisations.

5.1 Surface layer

The surface fluxes of momentum, sensible heat and water vapour are specified by

$$f_\alpha = C_D |V_k| (\alpha_k - \alpha_S)$$

where $\alpha = u, v, T, q$; k denotes values at lowest model level; S denotes surface values and $C_D = 2*10^{-3}$.

5.2 Planetary boundary layer

The parameterisation used is the same as that described by MANABE et al (1974). The flux divergences of u,v,q in the boundary layer are given by

$$\frac{\partial}{\partial z} K_v \frac{\partial \alpha}{\partial z} \qquad \alpha = u,v,q, \quad K_v = \ell^2 \frac{\partial v}{\partial z}$$

where $\ell^2(z)$ is specified by:

$$\begin{aligned} 0 \le z \le h \quad & \ell = k_o z \\ h \le z \le H \quad & \ell = k_o h\,(H-z)/(H-h) \\ H < z \quad & \ell = 0 \end{aligned}$$

where $k_o = .4$, $h = 75$ m, $H = 2.5$ km.

There is no explicit diffusion of T. Vertical transport of T in the boundary layer is assumed to be accomplished by the convection scheme.

5.3 Large scale condensation

This is assumed to occur if saturation occurs. The latent heat is released in situ and the condensate is immediately lost to the atmosphere as rain.

5.4 Convection

We used two different convection schemes due to MANABE and KUO.

5.4.1 MANABE Scheme (GARP 1974)

Convection occurs if the atmosphere is saturated and if the lapse rate exceeds the moist adiabatic lapse rate. If both these conditions occur then the temperature and humidity fields are adjusted so that the lapse rate is moist adiabatic, the air is saturated and the total internal plus latent energy is conserved. We note in particular that the convective rain can only occur in association with large scale rain.

5.4.2 KUO Scheme (KUO 1974)

In this scheme convection occurs if

(a) there is large scale convergence of moisture in boundary layer,

(b) the atmosphere is conditionally unstable.

When these conditions are satisfied the moisture convergence is partitioned between that part which increases the humidity of the column and that which is condensed in cumulus cloud.
The heating of the atmosphere due to convection is then proportional to the moisture convergence and the differences in q,T between the cloud and the environment.

5.5 Radiation

There was no radiative heating or cooling in the experiments.

5.6 Internal Dissipation

Two forms of internal dissipation were used, one non-linear due to SMAGORINSKY (1965) and the other a linear dissipation which is a modified form of the smoother introduced by SHAPIRO (1971).

5.6.1 Non-linear Dissipation

The tendency due to this term is written

$$\frac{\partial \alpha}{\partial t} = \frac{\partial}{\partial x} K_H \frac{\partial \alpha}{\partial x}$$

where $K_H = (2K, \Delta x)^2 \{ \left(\frac{\partial u}{x}\right)^2 + \left(\frac{\partial v}{x}\right)^2 \}^{\frac{1}{2}}$, $K_1 = 0.25$

5.6.2 Linear Dissipation

The linear filters introduced by SHAPIRO (1971) have been used by FRANCIS (1975) in a general circulation run . He used a 17 point filter in both directions. Such a filter is cumbersome

to use in the north south direction, as one needs to have 17 latitudes in core. The use of a 5-point filter would pose fewer problems in this area. One of the questions we examine in this report is whether a linear 5-point filter would prove suitable for the present integrations. The SHAPIRO 5-point filter is of the form

$$\overline{Z}_i^{\,1} = Z_i + S_1(Z_{i-1} - 2Z_i + Z_{i+1})$$

$$\overline{Z}_i = Z_i + S_2(\overline{Z}_{i-1}^{\,1} - 2\overline{Z}_i^{\,1} + \overline{Z}_{i+1}^{\,1})$$

where $S_1 = .25$
and $S_2 = -.25$.

The $\overline{Z}^{\,1}$ operator can be thought of as a smoothing operation and the final operation as a re-amplification.
The $\overline{Z}$ operator eliminates the 2 Δx wave. The coefficient is then chosen so that $\overline{Z}$ eliminates the two grid wave and has minimum effect on all other waves.

It is easy to show that

$$\overline{Z}_i^{\,1} = Z_i + (S_1 + S_2)(Z_{i-1} - 2Z_i + Z_{i+1}) + S_1 S_2 (Z_{i-2} - 4Z_{i-1} + 6Z_i - 4Z_{i+1} + Z_{i-2})$$

If we take $S_1 = S_2$ then the amplification factor on a Fourier mode $Z_j = e^{ikjx}$ is

$$1 - 16\,(S_1)\,\left(\sin^4 \frac{k\Delta x}{2}\right).$$

With $S_1 = 0.25$ the two grid wave $k = \frac{\pi}{\Delta x}$ is elimated. We found that this value of S_1 was rather too large and experimented with the values $S_1 = .1, .01$.

The 5-point SHAPIRO filter in one direction may be thought of as a ∇^4 operator. With our grid length and time step these values of S_1 correspond to values of 7×10^{16} and 7×10^{15} S.I. units for the coefficient of the ∇^4 operator.

5.7 The time filter (ASSELIN 1971) is used to damp the computational mode in time. We used the value 0.02 for the coefficient.

5.8 Dry convective diffusion

This scheme is similar to that used by CORBY et al (1972).

5.9 Dry adiabatic adjustment

This is similar in principle to the moist adiabatic adjustment, being invoked when the dry adiabat is exceeded.

6. Diabatic Integrations

Run with Planetary Boundary Layer (PBL), Surface Exchange-Processes (SL) and Dry Adiabatic Adjustment (DAD).

The adiabatic integration produces a very strong southward advection of cold air near the surface. After three days the temperature at the two lowest levels falls by over $20^{o}K$. If we allow the atmosphere to interact with the surface then this cold air will become dry adiabatically unstable.
The surface fluxes will quite readily dominate the advection in the lowest layer in the absence of the dry-adiabatic adjustment. This can be seen from the approximate thermal equation for the lowest layer,

$$\frac{\partial T}{\partial t} \sim - V \frac{\partial \bar{T}}{\partial y} - \frac{C_D |V| (\theta_N - \theta^*)}{\Delta z}$$

where θ_N is the potential temperature at the lowest level. θ^* is its surface value and Δz is the appropriate depth. Then a steady state solution is obtained if

$$(\theta_N - \theta^*) = \varepsilon \frac{\partial \bar{T}}{\partial y} \frac{\Delta z}{C_D} \qquad \text{where } \varepsilon \gtrless 1 \text{ as } V \gtrless 0 \ .$$

If we take $\frac{\partial \bar{T}}{\partial y} \sim 5^{o}K/400$ km, $z = 75$m, $C_D = 2*10^{-3}$

we see that $(\theta_N - \theta^*) \sim \varepsilon \ (0.5^{o}K)$ so that T at the lowest level will remain close to the value of T_*. If we make an integration with the surface fluxes but without the dry adiabatic adjustment we find that this is indeed the case but the computation breaks down after about 3 days due to the onset of dry convective instability.

In Fig. 9 we show the situation at day 3 in a run from day 0 with PBL, SL and DAD. A number of effects are immediately obvious. The kinetic energy generation is much reduced. The maxima and minima of V and T at the lowest layer have moved to the higher layers, to 926 mb for all but the temperature minimum in the cold air. This has moved upwards to 812 mb and the lapse rate below this minimum is very close to dry adiabatic. We note that the lowest layer (at 75 m) is some $7^{o}K$ colder than the underlying sea surface. Such air-sea temperature differences are common in cold air outbreaks. A rather undesirable feature of the results was that the humidity in the cold air tended to be concentrated in the lowest level with a value for q of .005 at 991 mb (r~ 80%) and .001 at 926 mb (r ~ 30%) where r is relative humidity. The vertical diffusion due to the boundary layer could not mix up the humidity fast enough to overcome the effect of the sinking motion and the horizontal advection. This seemed unrealistic in view of the strong vertical mixing of potential temperature that was occurring because of the dry advection. We therefore re-ran the experiment from day $1\frac{1}{2}$ with a diffusion scheme for dry convection which mixed θ and q at a rate proportional to the lapse rate

when it is dry convectively unstable. The differences in the fields of V, T are negligible. The lowest model layer in the cold air was dryer, q ~ .003 (r ~ 50%) and the value extended upwards to 800 mb (r ~ 100%).
In fact without this change none of the runs with large-scale rain and/or moist convection gave any precipitation in the cold air.

7. Runs with PBL, SL, Dry Diffusion, Large Scale Condensation and the Convection Schemes of KUO,MANABE

7.1 Logarithmic specification for $\partial q/\partial y$.

Since the model situation under study has an infinite source of energy the physical situations it produces are comparable with atmospheric values only in the early stages of the integration.
However, we can hope to identify systematic differences between physical parameterisations in these early stages. In the experiments to be reported here, there appears to be a definite tendency for the MANABE scheme to produce much sharper structures in the flow field than the KUO scheme, starting from the same smooth initial field.

The runs to be discussed now were all started from the state at day 1½ described earlier. We used a logarithmic humidity profile from day 1½. Fig. 3 shows the initial fields of V, T. Figs. 10, 11, 12 show the fields of V T at day 2, in three different runs : no convection scheme (Fig.10), MANABE scheme (Fig. 11), KUO scheme (Fig.12). Fig. 13 shows the accumulated total precipitation over the 24 hour period to day 2½ for these runs. In the first 18 hours of the period the KUO scheme produced more precipitation than the MANABE scheme, and both produce substantially more than the run without convection. In the last 6 hours of the period the relative positions are inverted.

After twelve hours, at day 2, there are marked differences in the V fields of the three runs. The maximum low level vorticities in the MANABE run are about twice as great as those in the other two runs which do not differ greatly among themselves in this respect. The patterns of $p^* \dot{\sigma}$ in these runs also show substantial differences after twelve hours (cf. Fig.14). The maximum value in the run without convection is .3Pa/sec. In the KUO run the pattern is very similar but the maximum is -.6Pa/sec. In the MANABE run the area of rising air is smaller by a factor of 2 and the largest vertical velocity is -1.8 Pa/sec. (65 mb/hour).

After 24 hours of integration the characteristics of the runs change somewhat. The vertical motion at the front intensifies considerably in all three runs as a result of the latent heat release. This intensification has been largest in the run without convection and least in the run with the KUO scheme.

This intensification is due to two effects : Firstly the convection schemes cool the lower layers and warm the upper layers compared to a run with no convection. This feature is commented on by MIYAKODA and SIRUTIS (1977). Secondly, the advection of q is dependent on the existing value of q. The combined effects are to produce more moisture convergence and higher temperatures at low levels in the run without convection. Consequently, when saturation is reached in the run without convection, much larger amounts of latent heat are released in a very narrow area.

The most significant stage of the integration for our purposes are the first twelve hours. Fig. 15 shows the pattern of total rainfall released in the 6 two hour periods between day 1½ and day 2 in the KUO and MANABE runs. Overall the KUO scheme has released 25% more precipitation. However,the pattern of latent heat release is quite different. The KUO scheme has a rate of .5 to 1mm/hr distributed over about 10 grid points throughout the period. The MANABE scheme has practically no precipitation during the first 6 hours and then a sharp increase to a maximum of 5mm/hour (average 2.5 mm/hour) at three or four grid points. This concentrated release of latent heat tends to accelerate the vertical velocity which in turn accentuates the latent heat release in a narrow area. The effect on the flow field is to produce in a two-hour period from day 1 hour 22 to day 2 hour 0 the marked change in the wind field shown in Fig. 16. This figure is the most surprising result of this work. One normally expects the geostrophic wind field to be affected by physical and dynamical processes on a time scale of about a day. These results show that a moderate amount of rainfall (5mm/hour) released in a localised fashion can cause rapid changes in the vorticity field, in certain circumstances.

7.2 Runs with linear specification for $\partial q/\partial y$.

One might object that these differences in behaviour of the schemes are sensitive either to the amount of precipitation being released or to the fact that the advection of moisture is proportional to the existing amount of moisture.

To test this point we started from the same initial conditions but with the north south gradient of q held constant. We made the restriction that q could not become negative.

During the first twelve hours to day 2 the KUO run releases about three times as much precipitation as the MANABE run, although the amounts are small. We look in detail at the period day 2 - day 2½. In the KUO run (Fig. 17a) in the first six hours precipitation is occurring at five points with an average value of about 1mm/2 hr. In the last six hours there is precipitation at 4 points but the average amount for these three increases to 2.5 mm/2 hours. In the MANABE run the precipitation sets in quite suddenly (cf.Fig. 17b). Between day 2 hour 4 and day 2 hour 6 there is about 4mm/2hr. at one point. During the next six hours there is precipitation at three points with a maximum rate of 10 mm/2hours.

At day 2 hour 12 the warm anomaly in both models has a very similar structure. There is a maximum at 926 mb, a relative minimum at 812 mb and a second relative maximum at 500 mb. On average the maxima and minima in the KUO scheme are about .45°K higher, consistent with the larger latent heat release. The fields of V (Fig.18) are rather more different. The vorticity at 812 mb is significantly larger near the front in the MANABE run. The patterns of $p^* \dot{\sigma}$ at day 2½ (Fig.19) are broadly similar. There is an intense rising motion at the vorticity maximum. A weak descending motion occurs behind it. There is a further weak region of rising motion to the west before the main body of sinking motion in the cold air. The secondary region of weak rising motion is well correlated in both runs with the region of large horizontal temperature gradient at 926 mb. However, the intensity of the rising motion at day 2½ is quite different between the runs. In the KUO runs the maximum velocity is at 664 mb with a value of -1.19 Pa/sec. In the MANABE run it is about double this value at -2.06 Pa/sec. The smaller region of weakly descending air has a maximum velocity of .14 Pa/sec. in the KUO run and .16 Pa/sec. in the MANABE run. The secondary region of rising air has a different structure between the runs. In the MANABE run there is a maximum at mid levels of -.15 Pa/sec. In the KUO run the maximum occurs at 926 mb with a value of -.05 Pa/sec.

At day 3 in these runs qualitatively similar differences are to be found in the vertical velocity field, with the MANABE scheme having a maximum value of -1.8 Pa/sec. and the KUO run showing a value of -.12 Pa/sec. A similar comment may be made about the weak secondary rising motion. The temperature and V fields, however, show smaller differences than they did at day 2½.

7.3 Summary

To summarise then, the inception of precipitation in runs with the MANABE and KUO schemes is rather different. With the KUO scheme the inception is a gradual process with a slow build up in the vertical circulation associated with the front. In the MANABE scheme on the other hand the process is sudden. The precipitation is more concentrated and has larger values, about double those in the KUO scheme. The vertical circulation at the front is much stronger by a factor of 1.5 to 2. The initial effects on the vorticity field are to produce sharper vorticity maxima.

Our conclusions about the differences between the schemes in the run with a logarithmic specification for $\bar{q}$ are borne out in the run with a linear specification for $\bar{q}$. Given the nature of the MANABE scheme, which does not permit convection until saturation is reached, one would expect the onset of precipitation to be sudden. What is interesting about the present results are the consequences of the sudden onset for the flow field. There is a sharp intensification of both the vertical velocity and the vorticity and the scale on which this occurs is initially smaller than in the runs with the KUO scheme.

8. The further Development of the Frontal Systems

The further development of the frontal system in these integrations is of some interest. The relevance of the evolution to the atmosphere is perhaps in doubt because the character of the evolution is dominated by the infinite energy source available to the two-dimensional model. Nevertheless it does provide an interesting if extreme example of the effect of latent heat release on frontal development.

8.1 Dry model

In the adiabatic integration, at day 3, about 12 hours before the model blew up we can see (cf. Fig.4) that the regions of sharpest gradient in T and V at the lowest layer are tending to become coincident. This agrees with the analytic results of HOSKINS and BRETHERTON (1972).

In the run with just PBL, SL and DAD (Fig. 8) at day 3, a similar comment may be made. In this run the comment applies to the level at 926 mb.

8.2 Runs with linear specification of $\partial\bar{q}/\partial y$

In the runs with convection and a linear profile for the basic state humidity events do not follow the same pattern. In the MANABE run at day $3\frac{1}{2}$ (Fig.20) there are two low-level vorticity maxima. The larger by far occurs at the main front. The weaker vorticity maximum is well correlated with the zero perturbation isotherm at 926 mb. The maximum horizontal temperature gradient at this level occurs close to this isotherm. This is also the place where the weak secondary region of rising air occurs. There is in addition, in this region, a weak maximum in precipitation. Moreover, the largest temperature gradients at 926 mb occur in the same place where the dry convection in the cold air is beginning to transport heat away from the surface.

Fig. 21 shows the fields of p* and V T at the lowest model level in this run. There is a temperature change of $3^{o}K$ at the main vorticity maximum with a larger change occurring at the weak vorticity maximum. To the west of this point lies the main body of cold air. We note too the slight change in the gradient of p* at this point. Taking all these points together it would seem not unreasonable to describe the feature as a secondary front.

In the run with the KUO scheme and a linear $\bar{q}$ profile in the basic state (Fig.22) the V field at day $3\frac{1}{2}$ is different from the MANABE run as there is no secondary vorticity maximum. The T field is rather similar in the two runs. The secondary peak of rising motion is weaker by a factor of 5. There is no secondary peak in the rainfall and there is no secondary vorticity maximum. These points are of course intimately related.

From the onset of the precipitation in each run with a linear specification for $\bar{q}$ two cells of rising motion were apparent. We have no theoretical explanation for this fact. The cells in the MANABE run were stronger. Presumably the weaker of the two cells in the MANABE run was sufficiently intense to induce precipitation which reinforced the vertical motion and led to the secondary vorticity maximum.

Our interpretation of this secondary vorticity maximum as a weak secondary cold front is not in serious disagreement with the definition given by McINTOSH (1972) : " The development of a trough or troughs of low pressure within the cold air mass lying in the rear of a deep depression is relatively common. On those occasions on which a trough appears to mark the line of advance of colder air (owing to rather different recent histories of the air masses on either side of the trough) the trough line is termed a secondary cold front".

The system under discussion has many of the features mentioned in McINTOSH's definition. There is a deep low, the main body of cold air is well to the rear of the main vorticity maximum or main cold front; there is dry convection in the coldest air; near the zero-perturbation isotherm there is moist convection. In the run with the MANABE scheme the convection is intense enough (and localised enough) to sustain a vertical circulation; this vertical circulation is sufficiently strong to generate a marked vorticity maximum which is associated with a change in the pressure gradient.

8.3 Runs with logarithmic specification for $\partial\bar{q}/\partial y$

The evolution in the runs with the logarithmic profile for $\bar{q}$ was different yet again. In the MANABE run (Fig. 23) the latent heat release and the associated vertical velocities at day 3, near the main front, were sufficiently strong to induce much larger southward velocities just behind the main front. The strong associated cold air advection changes the temperature field so that the main thermal gradient at low levels is now much more closely associated with the main vorticity maximum.

In the KUO run at day 3 the southward velocities are not so large, 17 m/s as against 25 m/sec., so that the sharpening of the thermal gradient near the vorticity maximum has not yet occurred. By day $3\frac{1}{2}$, however, this change has taken place and the thermal pattern then looks very similar to that in the MANABE run.

In both these runs the secondary region of rising air is weaker than in the runs with a linear humidity gradient. As a consequence the secondary vorticity maximum is weaker and there is no secondary rainfall peak.

These examples, although rather extreme, show that latent heat release can have significant effects on the dynamical evolution of baroclinic waves.

9. Internal Dissipation

Internal dissipation is used in numerical models of the atmosphere for two reasons; to control computational noise and to represent the dissipation that occurs on unresolved scales. Linear dissipation is not generally favoured. For practical reasons it can only be used as a second order or at most, fourth order smoother, due to core store limitations. Second order linear dissipation has a severe damping effect on all wave-lengths if it is strong enough to control the noise. A fourth order smoother, such as we have used here is much more selective. For example,

$$K_4 \frac{d^4}{dx} \text{ and } K_2 \frac{d^2}{dx^2}$$

have the same effect on a four-grid wave if $K_4 = 7 \times 10^{16}$ and $K_2 = 6 \times 10^5$, all units S.I. Table 2 shows the e-folding time in days for the four longest waves when wave number 1 is represented by 48 points and $\Delta x = 106$ km, for these values of K_4, K_2 .

Wave Number	Fourth Order	Second Order
1	71.16	.61
2	4.48	.15
3	.90	.07
4	.29	.04.

TABLE 2

The table shows clearly the greater selectivity of the fourth order operator.

Storage considerations make it difficult to implement smoothers of higher than second order in a three-dimensional model. FRANCIS (1975) however used a linear Shapiro filter of order 16 and found a large increase in the eddy kinetic energy of a general circulation run.

Non-linear smoothing operators have quite different effects on the spectrum as compared with linear smoothers. Non-linear operators tend to localise their effects to regions of large gradients in physical space. Thus there is no a-priori reason which limits their effects, by and large, to the short wave end of the spectrum. Preliminary experiments, to be reported elsewhere, show that non-linear smoothers tend to preserve the shape of the spectrum while reducing amplitudes at all wave numbers. Linear filters on the other hand suppress the short wave end of the spectrum while leaving the long wave end nearly untouched.

The value of $K_4 = 7 \times 10^{16}$ which we used in the experiments described above is larger than we would want to use in practise. If we repeat the experiments with $K_4 = 7 \times 10^{15}$ there is very little difference in the overall features of T, V except that the fields are somewhat rougher. However, the vertical velocity field is so noisy that one would need to smooth it in time in order to be able to distinguish the main areas of rising or sinking motion.

As a measure of this noise we calculated the ratio R_1 of the divergent energy (u component energy) in wave numbers 2 - 11 to the divergent energy in wave number 1, and the ratio R_2 of the divergent energy in wave numbers 12 - 24 to the divergent energy in wave numbers 2 - 11. Fig. 24 shows the values of R_1, R_2 for three runs with the MANABE scheme using the linear specification for $\partial\bar{q}/\partial y$. These runs were with the non-linear SMAGORINSKY diffusion and with two values of K_4, (7×10^{15}, 7×10^{16}) with the linear ∇^4 operator. Fig. 25 shows results from similar runs when the KUO scheme is used. In all runs the ratio R_1 is relatively unaffected by the smoothing operator. The ratio R_2, on the other hand, is quite sensitive to the smoothing. The runs with non-linear diffusion and with $K_4 = 7 \times 10^{15}$ show similar values of R_2 while the runs with $K_4 = 7 \times 10^{16}$ show much reduced values of R_2. The run with the KUO scheme shows values of R_2 about half that in the run with the MANABE scheme. We note too the smoother growth of R_1 in the KUO run as compared with the rapid jump with the onset of precipitation at day 2 in the MANABE run.

The fact that the MANABE scheme produces significant computational noise is of course well known (MIYAKODA et al 1977).

10. Summary and Conclusions

The results presented above show that there are significant differences in the behaviour of the moist convection schemes. In general the KUO scheme has a smoother and more gradual effect on the integrations as compared with the MANABE scheme.

The use of a dry adiabatic adjustment or a diffusive representation for dry convection has little effect on the integrations presented here. However, the vertical transport of moisture by dry convection is probably important in cold outbreaks.

The linear ∇^4operator with a coefficient of 7×10^{16} m^4/s gave smooth vertical velocity fields. A weaker value of 7×10^{15} in the linear dissipation, or a non-linear dissipation of the form introduced by SMAGORINSKY with k = 0.25 (MIYAKODA 1973) gave rather similar results for the shortest waves in the divergence field.

The formulation of the internal dissipation is known to have a profound effect on numerical forecasts. The present experiments because of their idealised nature and short time span are of little help in choosing a formulation.

Up to this point we have confined the discussion of the Manabe and Kuo schemes to a comparison of their performance in idealised situations. We have not considered which of them might be more realistic in comparison with the real atmosphere. For tropical regions that has been a matter of lively debate (KRISHNAMURTI 1969, CESELSKI 1973, MIYAKODA and SIRUTIS 1977). In mid latitudes a modified version of the Manabe scheme has been in operational use for several years (BENWELL and BUSHBY 1970). Forecasting experience with the Kuo scheme is much more limited (EDMON and VINCENT 1976, HAMMARSTRAND 1976). These latter results appear quite promising as compared with the Manabe scheme. The present work also indicates that the Kuo scheme has some computational advantages over the Manabe scheme. Thus, although it is premature to draw conclusions, there are indications that an extensive trial of the Kuo scheme would be useful.

Finally, we have found that these experiments with a two-dimensional model provide a cheap way of testing codes for inclusion in a three-dimensional model and shed useful light on some aspects of the behaviour of the parameterisations.

References:

Asselin, R. 1972 Frequency filter for time integrations. Mo.Wea. Rev. 100, 487-490.

Benwell, G.R.R. and F.H. Bushby 1970 A case study of frontal behaviour using a 10-level primitive equation model. Quart.J.Roy.Met. Soc. 96, 287-296.

Burridge, D.M. 1977 A model for medium range weather forecasts - Adiabatic Formulation. Technical Report No. 4,ECMWF,46 pp.

Ceselski, B.F. 1973 A comparison of cumulus parameterisation techniques. Tellus 25 ,459-478.

Charney, J.G. 1947 The dynamics of long waves in a baroclinic westerly current. J. Meteor. 4, 135-162.

Corby, G.A. et al 1972 A general circulation model of the atmosphere suitable for long period integrations. Q.J.Roy. Met. Soc. 98 ,809-832.

Eady, E.T. 1949 Long waves and cyclone waves. Tellus 1, 33-52.

Edmon H.J. and D.G. Vincent 1976 An application of two tropical Parameterisation Schemes of Convective Heat Release in Middle Latitudes. Mon. Weath. Rev. 104, 1141-1153.

Francis, P.E. 1975 The use of a multipoint filter as a dissipative mechanism in a numerical model of the general circulation of the atmosphere. Quart.J.Roy.Met. Soc. 101, 597

GARP 1974 Modelling for the first GARP global experiment. GARP Publication Series No.14. WMO-ICSU Joint Organising Committee.

Hammarstrand, U. 1976 On parameterisation of convection for large scale numerical forecasts at mid-latitudes. Proc. Int.Conf. on Simulation of Large-Scale Atmospheric Processes, Annalen der Meteorologie (N.F.) Nr. 11, Deutscher Wetterdienst.

References:

Hollingsworth, A. 1976 Two-grid waves associated with the finite difference form of the hydrostatic equation. Unpublished.

Hoskins, B.J. Bretherton, F.P. 1972 Atmospheric Frontogenesis Models. Mathematical Formulation and Solution. J.Atmos.Sci. 29, 11-37.

Hoskins, B.J. 1971 Atmospheric Frontogenesis: Some Solutions. Quart.J.Roy.Met. Soc. 97, 139-153.

Krishnamurti, T.N. 1969 An experiment in numerical prediction in equatorial latitudes. Quart. J. Roy. Met. Soc. 95, 594-620.

Kuo, H.L. 1974 Further studies of the parameterisation of the influence of cumulus convection on large-scale flow. J.Atmos.Sci. 31, 1232-1240.

Manabe, S. et al 1965 Simulated Climatology of a general circulation model with a hydrological cycle. Monthly Weather Review. 93, 769-798.

McIntosh, E. 1972 Meteorological Glossary. London H.M.S.O. 319 pp.

Miyakoda, K. 1973 Cumulative Results of testing a Meteorological Mathematical Model - The description of the model. Proc. Royal Irish Acad. 73, A9

Miyakoda, K. and J. Sirutis 1977 Comparative Integrations of Global Models with various parameterized processes of sub-grid scale vertical transports: Description of the parameterisations and preliminary results. To be published.

References:

Shapiro, R. 1970 Smoothing Filtering and boundary effects. Rev.Geophys. Space Phys. 8, 359-387.

Smagorinsky, J. et al 1965 Numerical Results from a nine level general circulation model of the atmosphere. Mo. Wea. Fev. 93, 727-768.

Williams, R.T. 1967 Atmospheric Frontogenesis: A numerical experiment. J. Atmos. Sci. 24, 627-641.

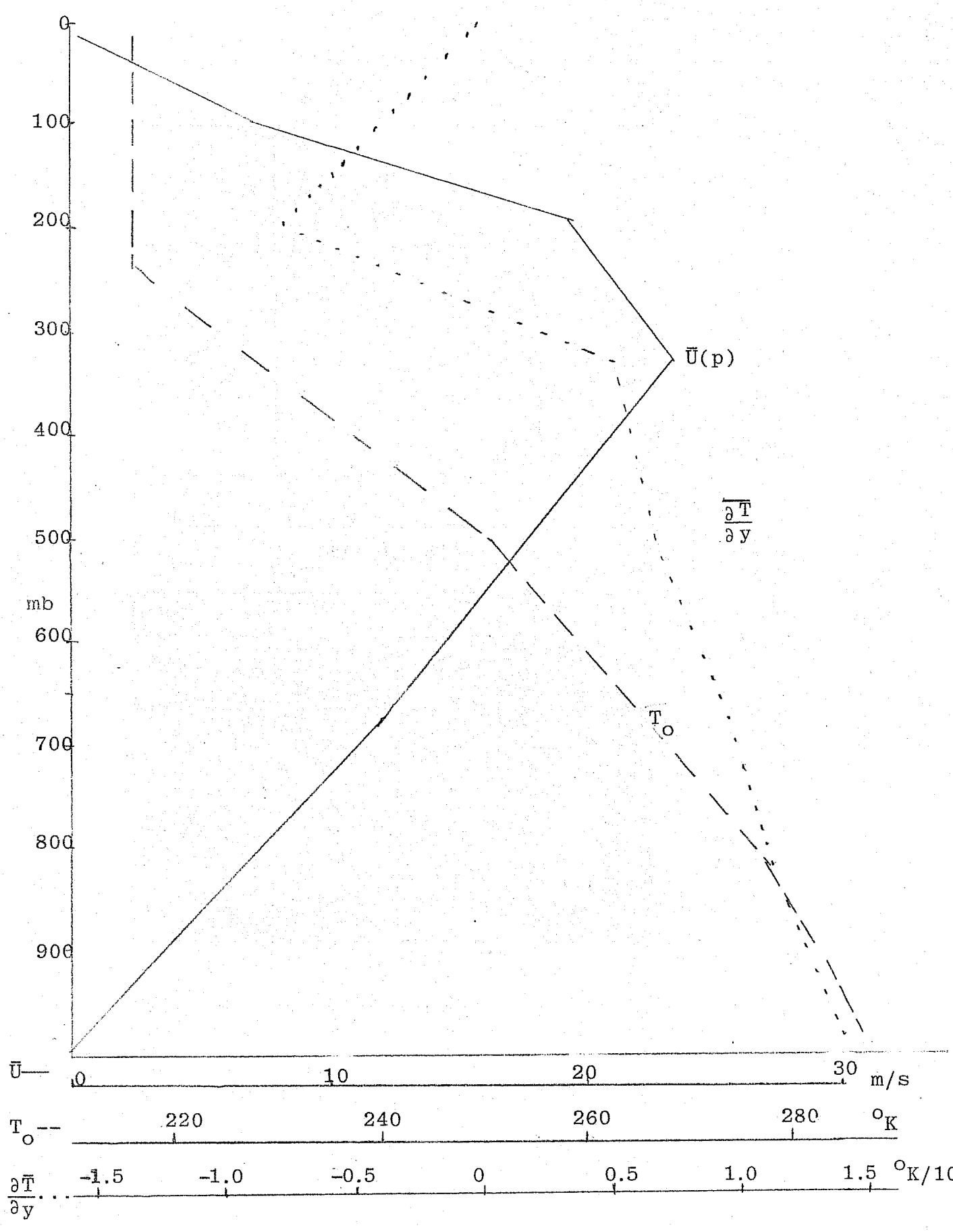

Fig. 1 $\frac{\partial \bar{T}}{\partial y}$, $\bar{U}$, and T_o, as functions of pressure. $\frac{\partial \bar{T}}{\partial y}$ is held constant during the integration. $\bar{U}$ is the corresponding geostrophic wind. T_o is taken from ICAO standard atmosphere and is the zonally averaged temperature field initially.

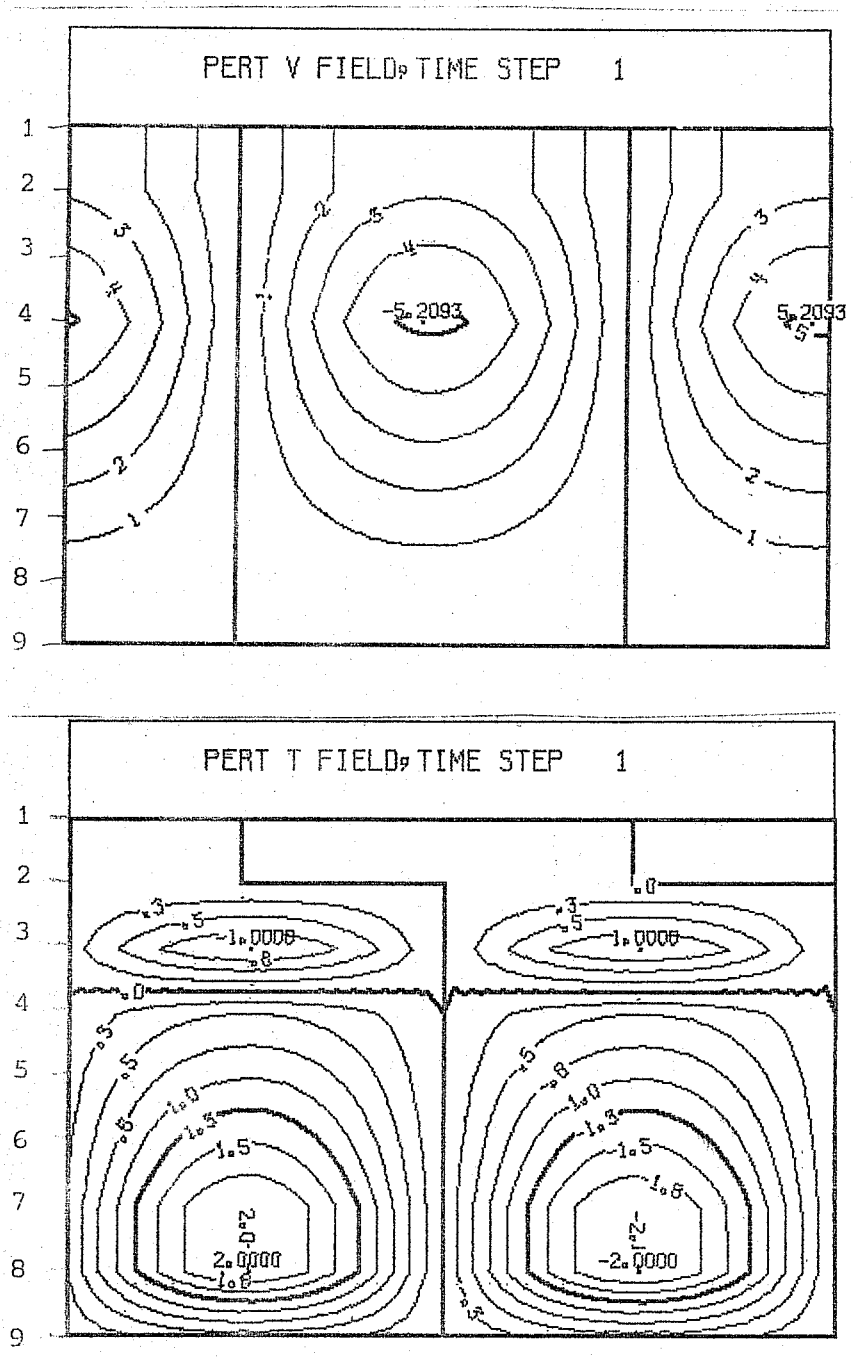

Fig. 2 (x,σ) plots of V',T' after one time step. These and all the following plots, treat the σ-levels as equally spaced in the vertical. The number of the level corresponds to the pressure levels in Table 1 if the surface pressure is 1000 mb. This representation was chosen to exhibit the details of the motion near the lower boundary. V' positive is northward. T' is the departure of T from its mean state at t = 0, i.e. T_o of Fig. 1. The local maxima and minima are indicated.

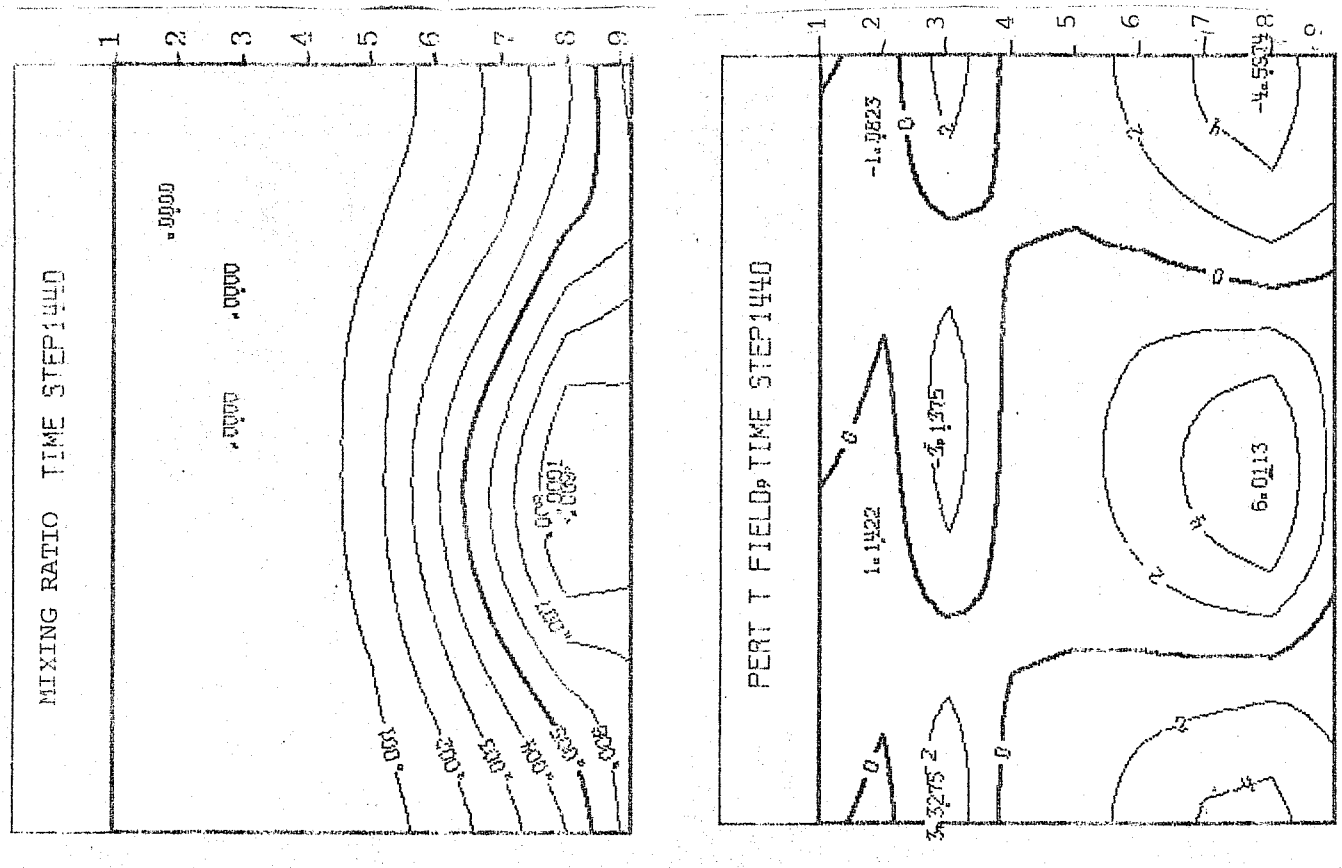

Fig. 3 Fields of q,V',T' at day 1½. Integration started from Fig. 2 with parameterizations for planetary boundary layer, surface layer, large scale condensation and linear ∇^4 dissipation $K_4 = 7 \times 10^{15}$. Vertical scale as described in Fig. 2.

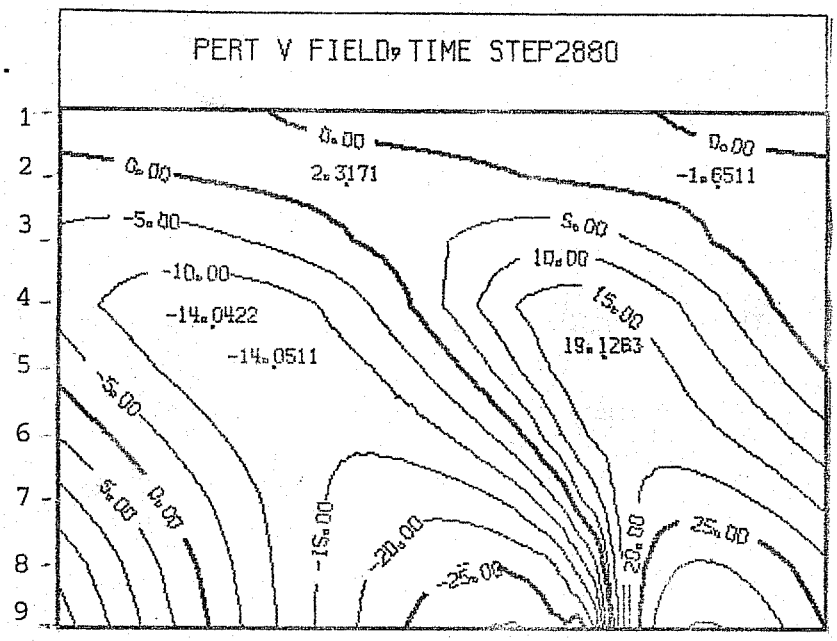

b.

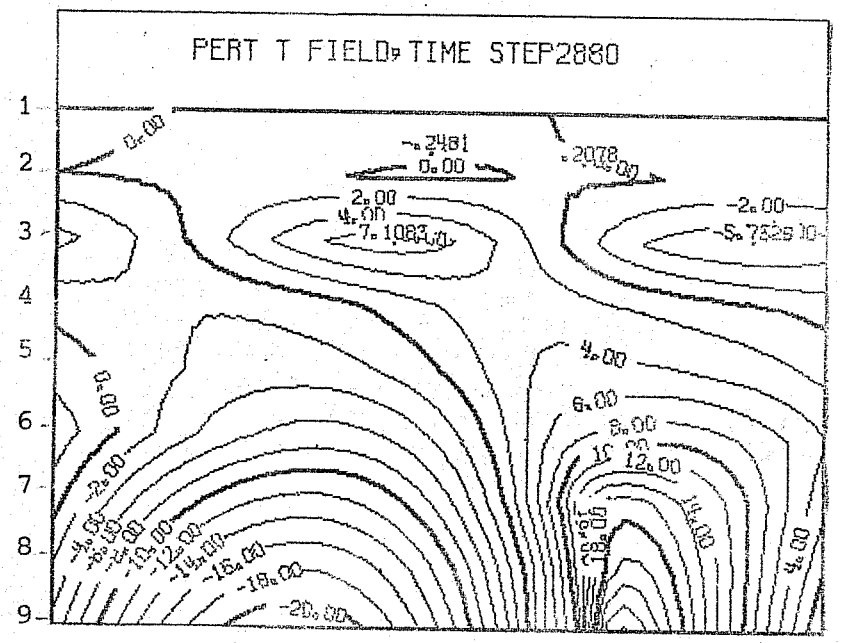

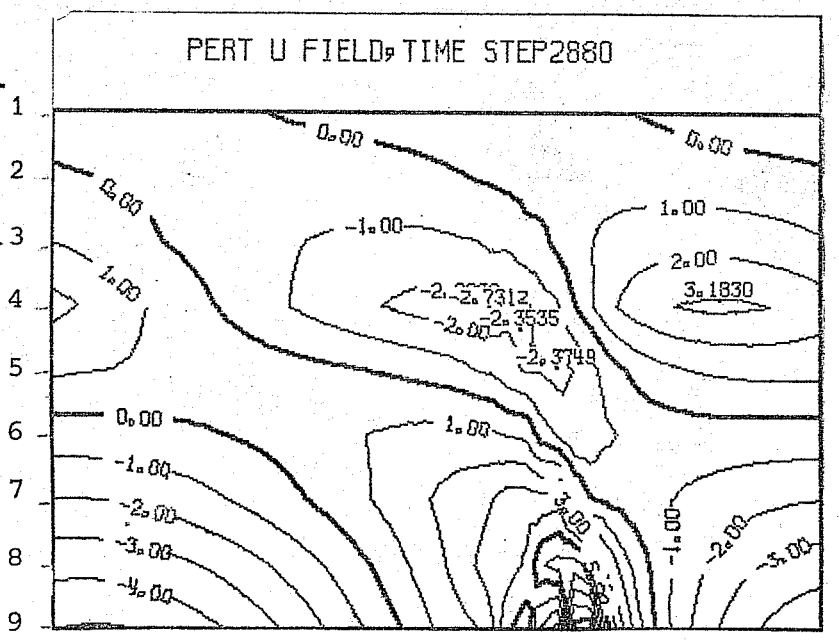

Fig. 4 Fields of V',T',U' in the adiabatic integration at day 3 starting from Fig. 2. See Fig. 2 for vertical scale. The units are m/sec, °K, m/sec.

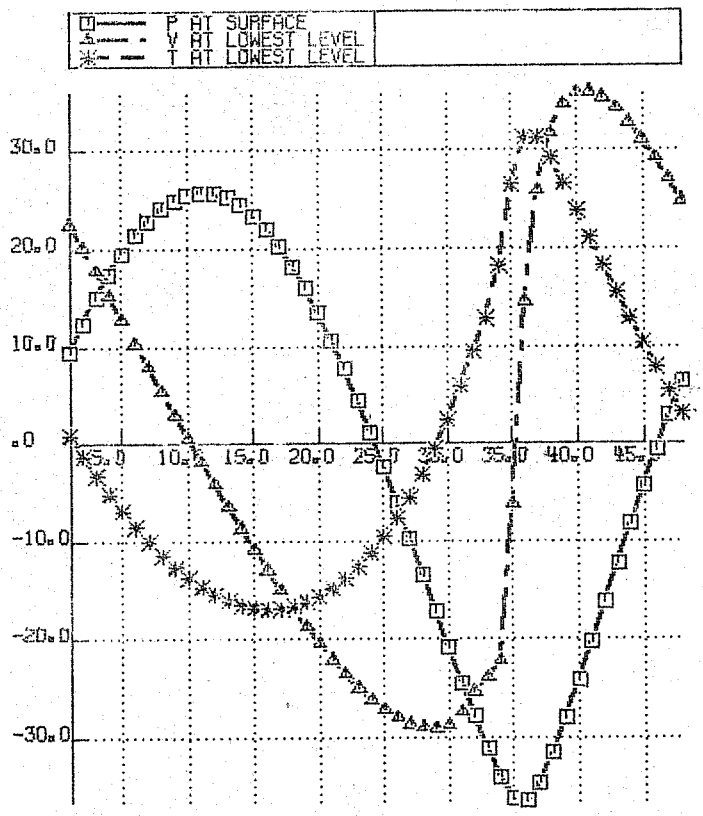

Fig. 5 Zonal profiles of p* (□), V_9 (Δ) T_9 (*) at day 3 in the adiabatic integration shown in Fig. 4. The scale on the left applies to all three quantities, the units being respectively Hectopascals (mb), m/sec, °K. The horizontal scale gives the grid point number (48 in all).

a.

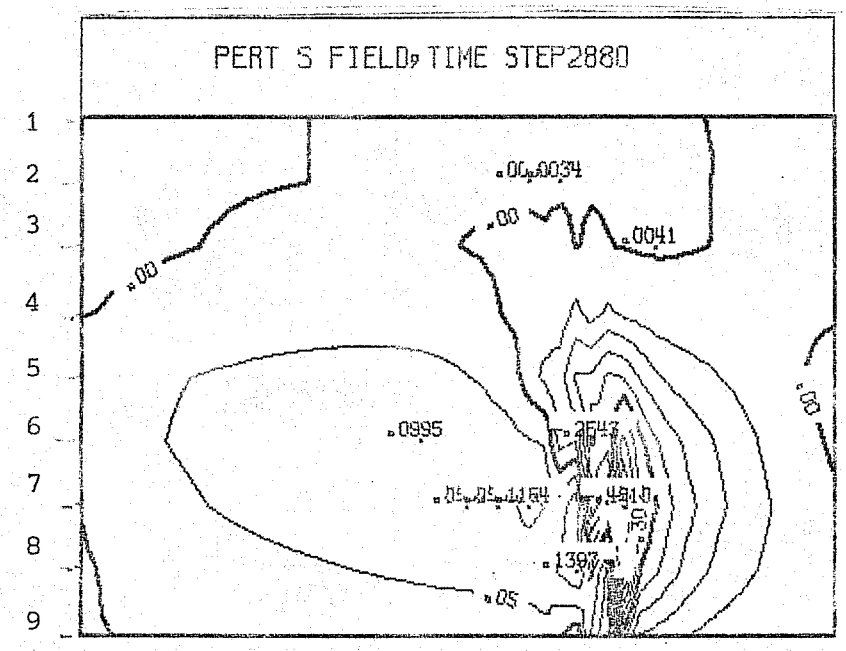

b.

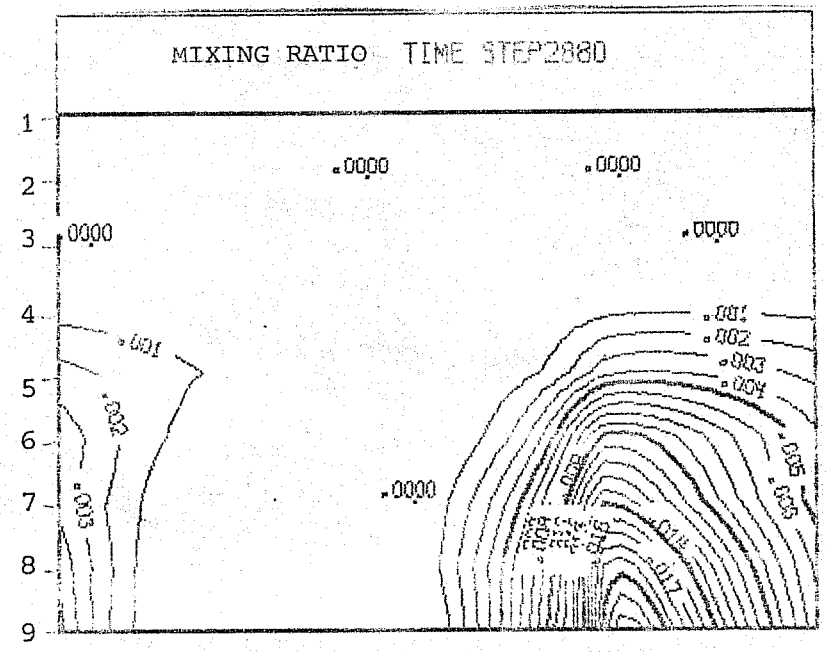

Fig. 6 a, b Fields of $p^*\dot{\sigma}$, q at day 3 in the adiabatic integration. The units are Pa/sec and gm/gm. See Fig. 2 for vertical scale.

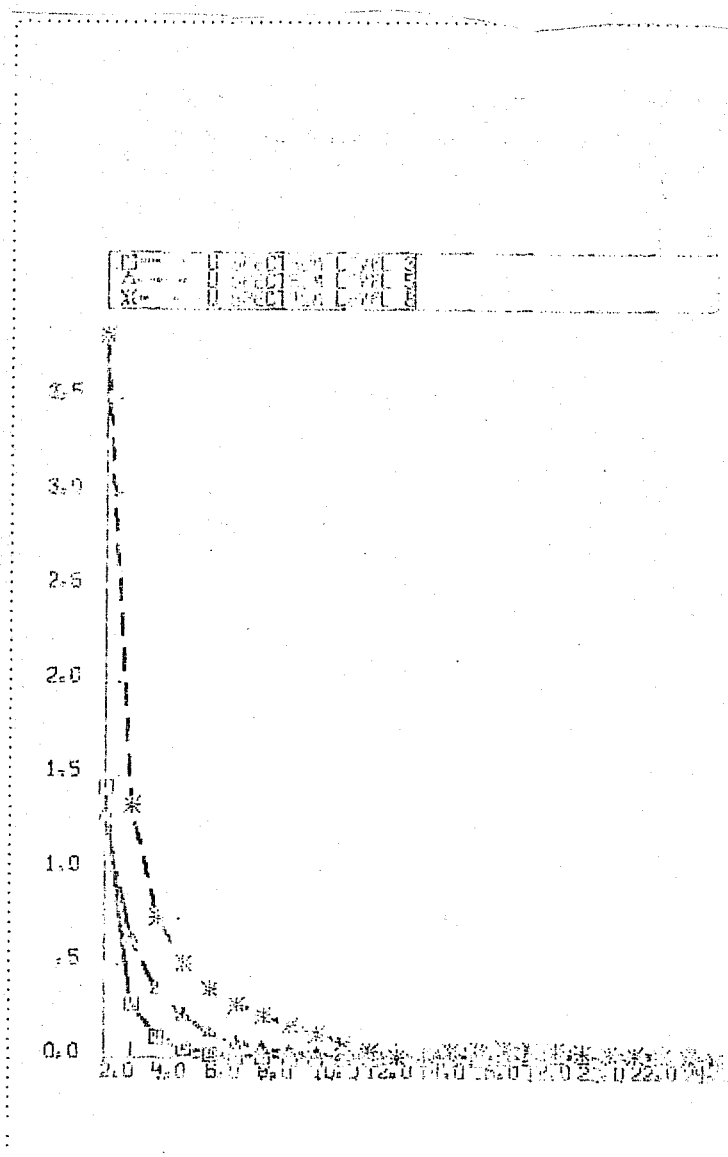

Fig. 7 Longitudinal spectra (for wave numbers 1-24) of u at levels 3,5,8 at day 3 in the adiabatic integration. The units are m/sec. (□ level 3, Δ level 5, * level 8).

a.

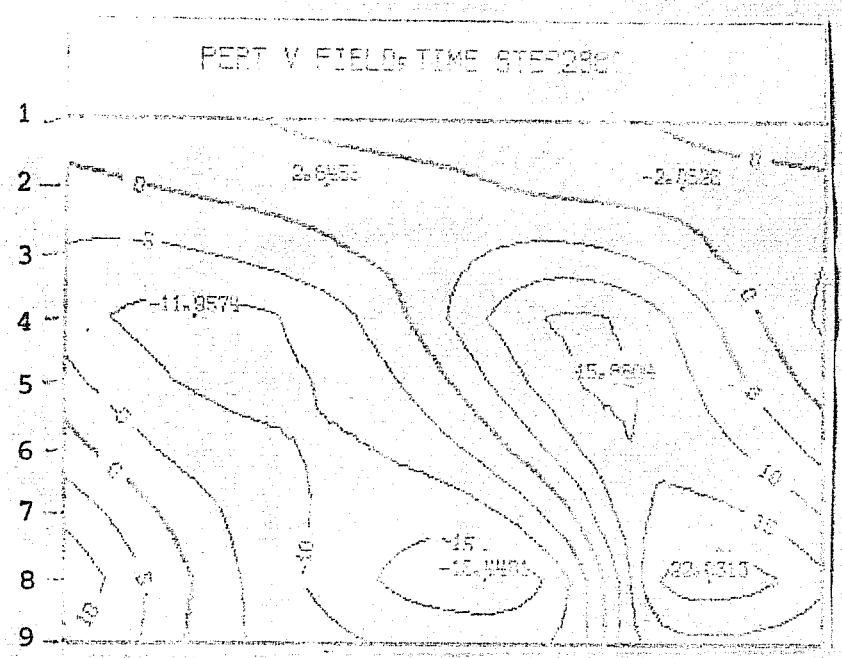

b.

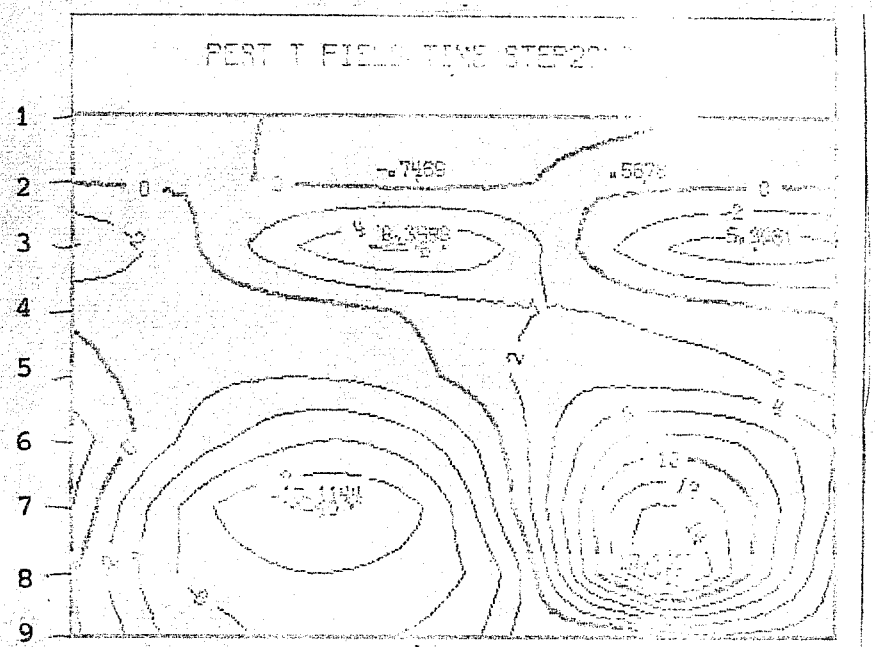

c.

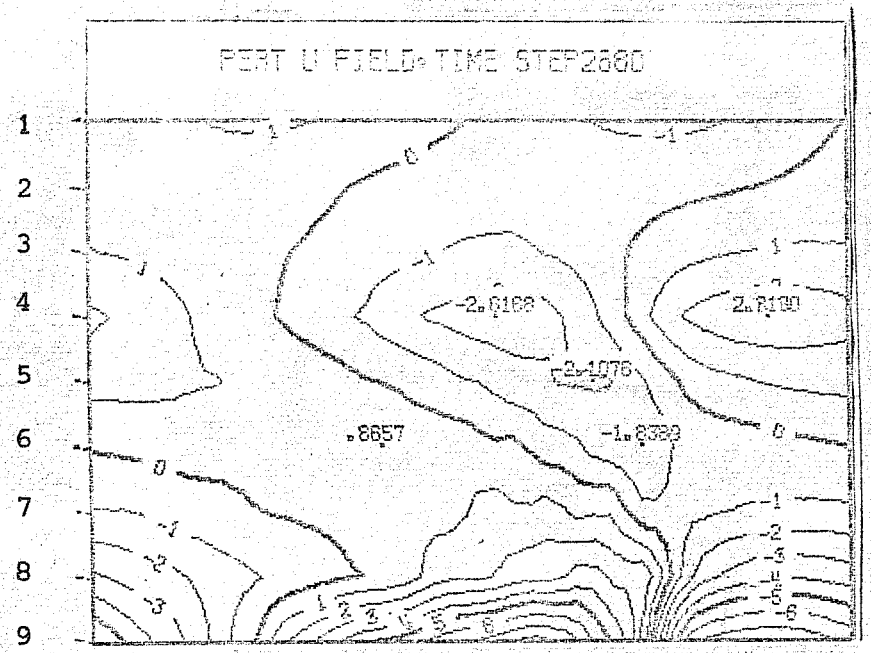

Fig. 8 The fields of V',T', u' at day 3 in the run with PBL, SL, DAD. The units are m/sec, ^{o}K, m/sec. See Fig. 2 for vertical scale.

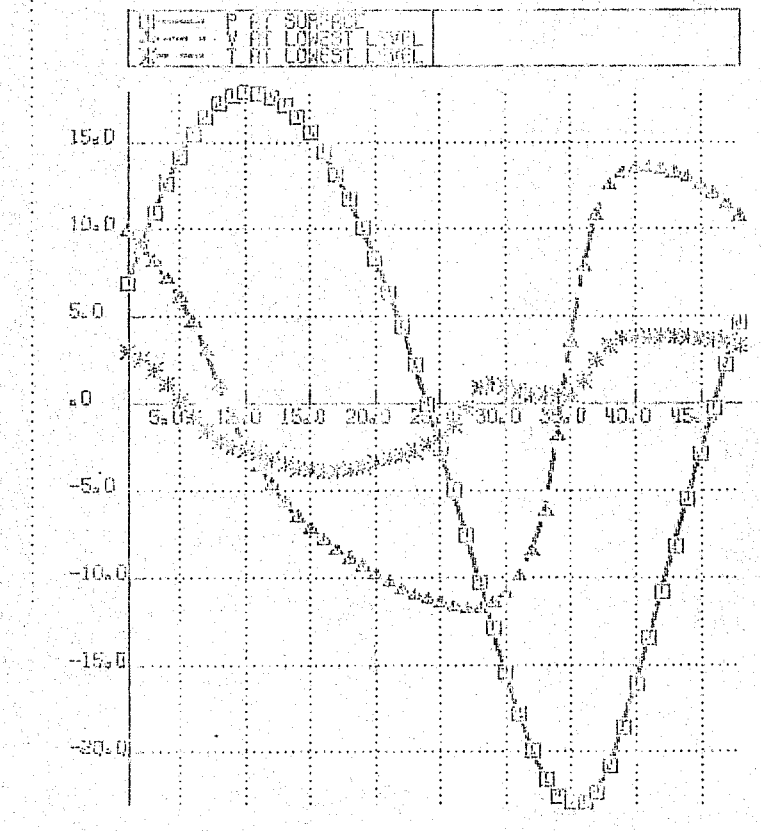

Fig. 9 Zonal profiles of P* (□), V_9 (Δ), T_9 (*) at day 3 in the run with PBL, SL, DAD. The units are HPa, m/sec., ^{o}K.

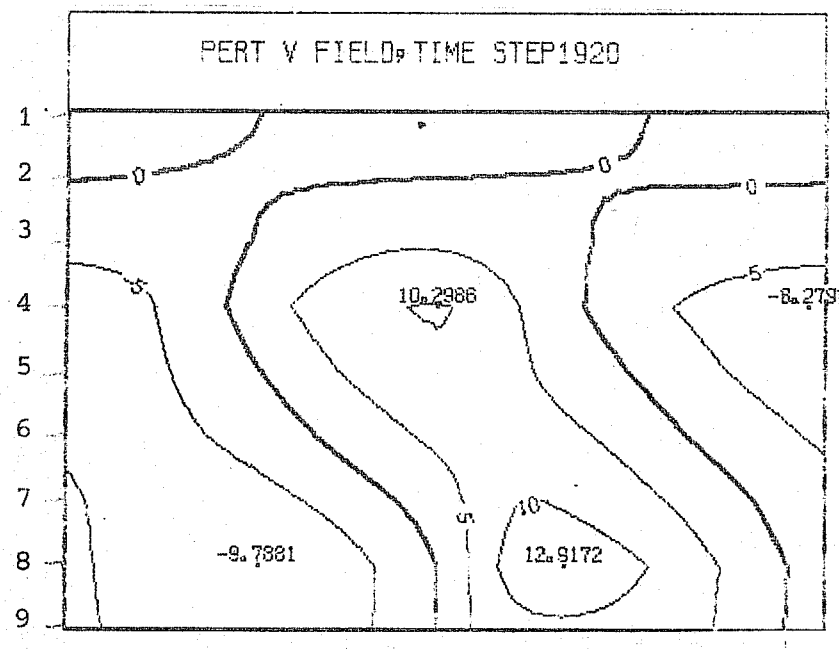

a.

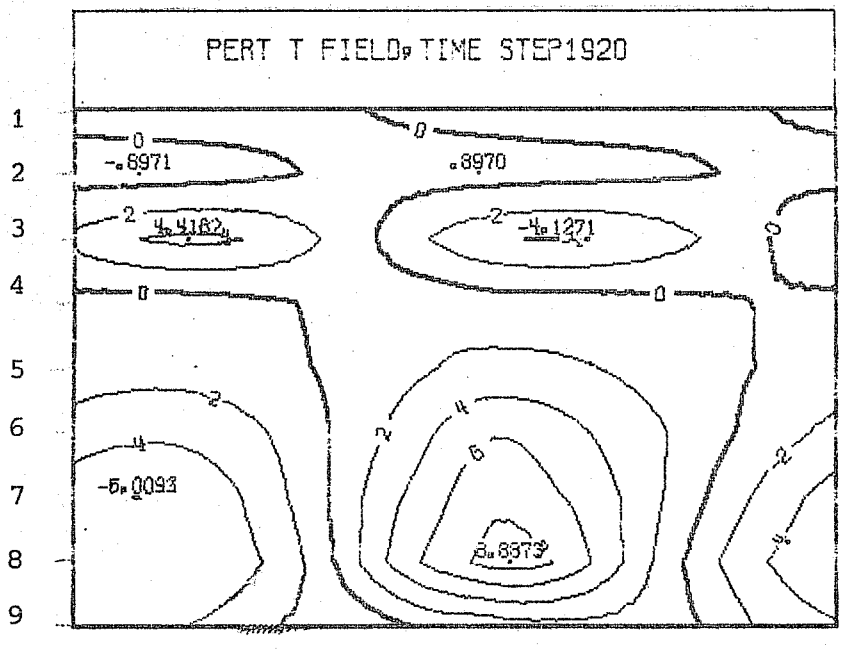

b.

Fig. 10 Fields of V',T' after 12 hours (i.e. day 2 Fig.10a) and 24 hours (i.e. day 2½, Fig.10b) integration from state shown in Fig. 3, using a logarithmic specification for $\frac{\partial q}{\partial y}$. The parameterisations used were PBL, SL, large scale condensation, diffusive dry convection and $K\nabla^4$ dissipation with $K_4 = 7 \times 10^{16}$.
See Fig. 2 for vertical scale.

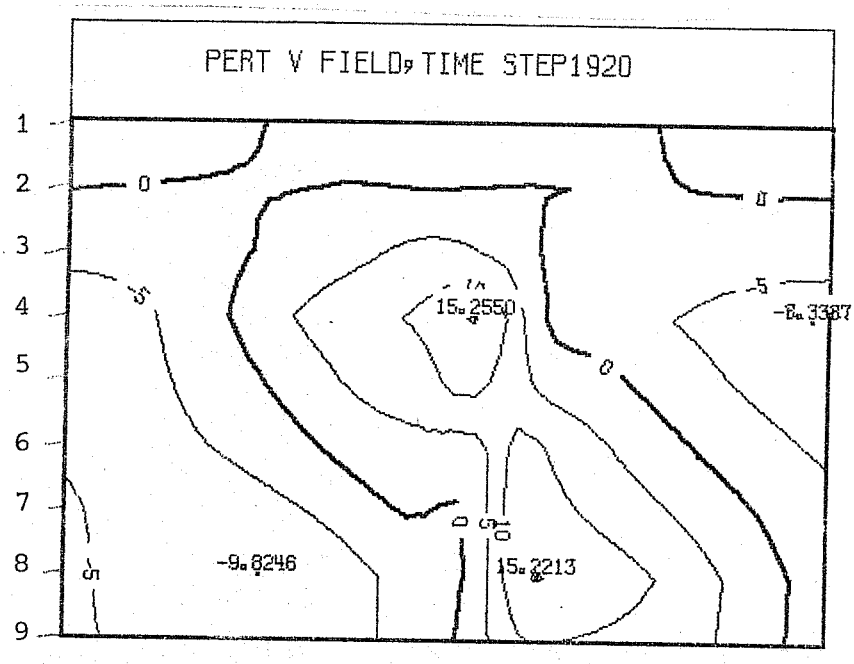

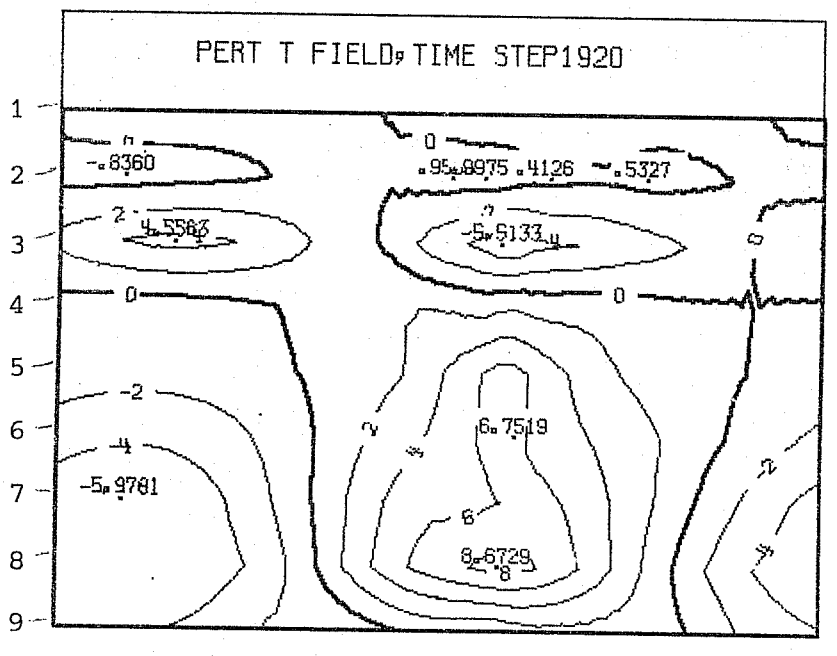

Fig. 11 As Fig.10 (a,b) except that the effect of the Manabe convection scheme has been included.

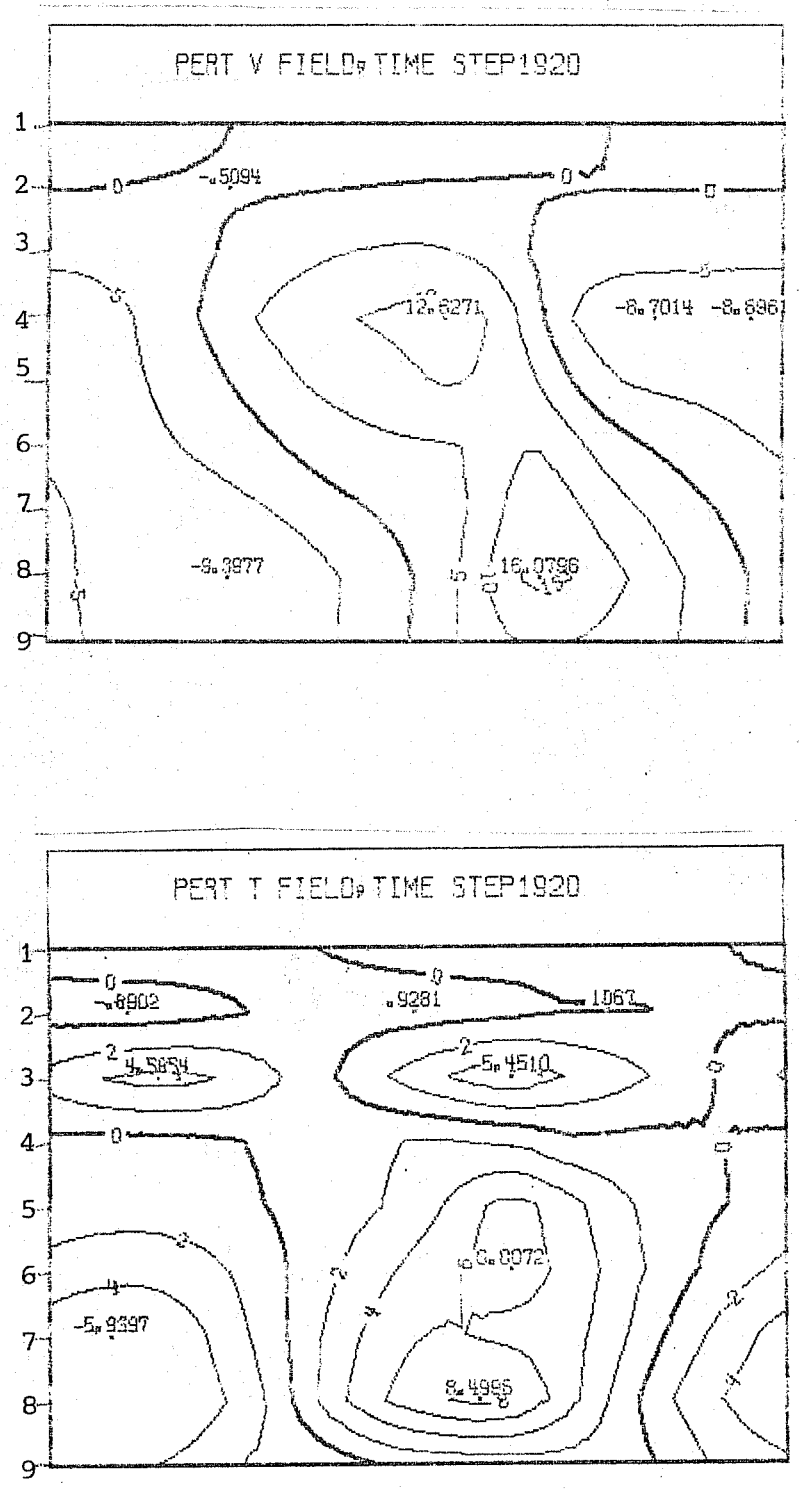

Fig. 12 As Fig. 10 (a,b) except that the effect of the Kuo convection scheme has been included.

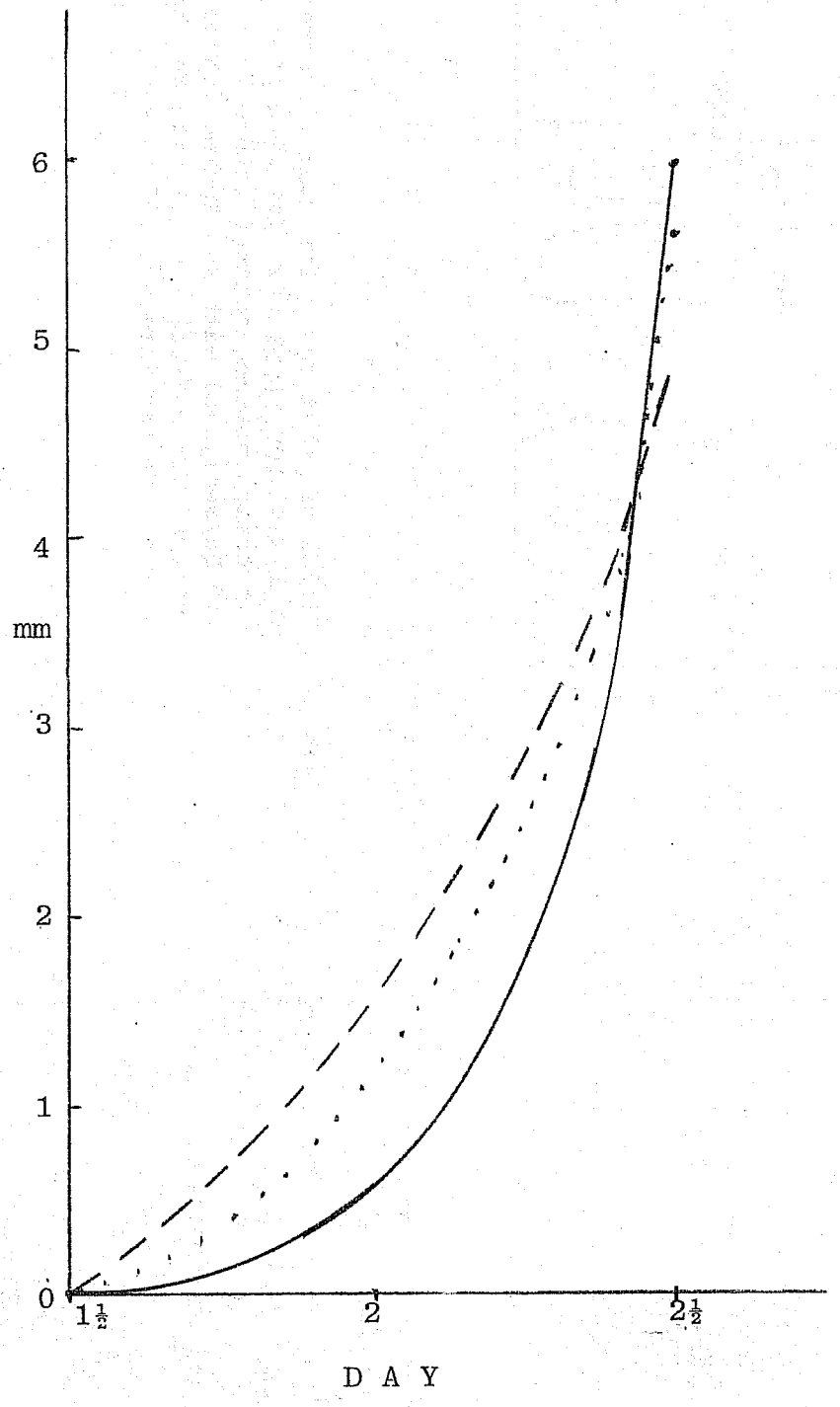

Fig. 13 Total accumulated precipitation between day 1½ and 2½, averaged over the domain, for the runs illustrated in Figs. 10, 11, 12 respectively with no convection scheme (-), with Kuo scheme (--), with Manabe scheme (...). The units are mm.

a.

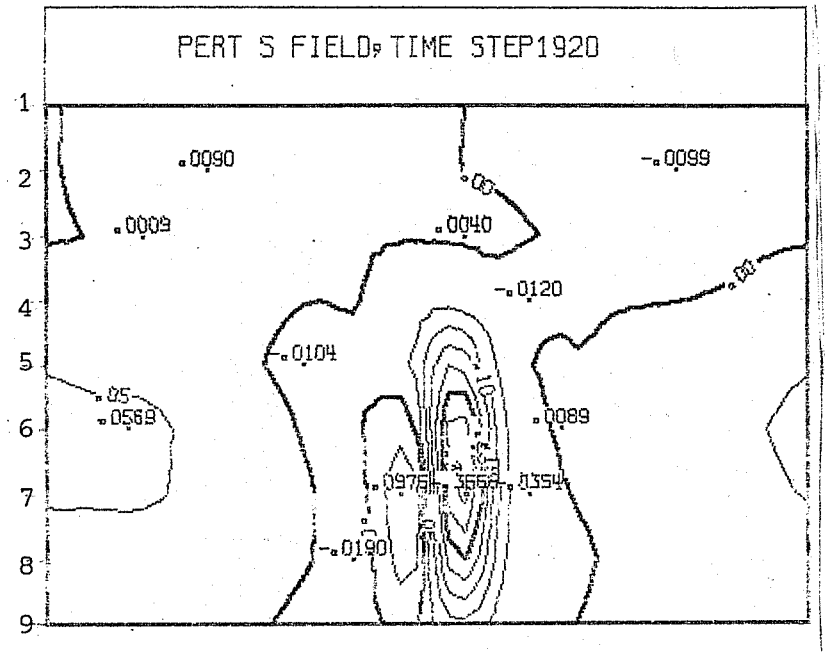

b.

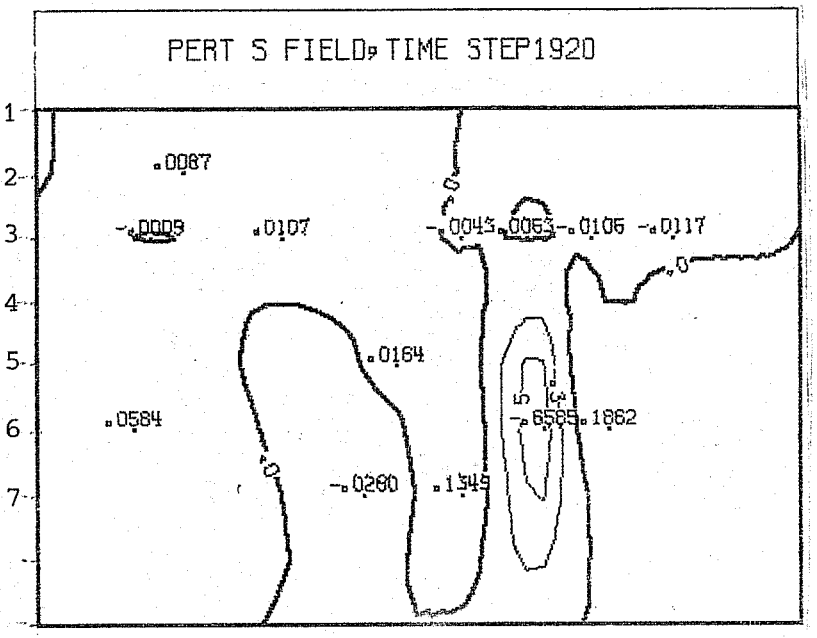

c.

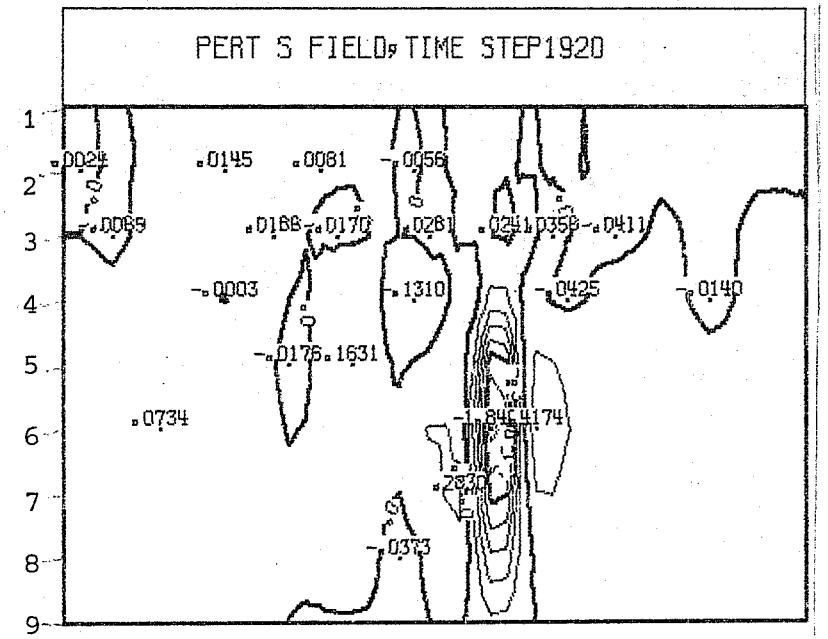

Fig. 14 Fields of $p^*\dot{\sigma}$ at day 2 for runs illustrated in Figs. 10, 11,12 viz. (a) with no convection scheme (contour interval .05 Pa/sec), (b) with Kuo scheme (contour interval .25 Pa/sec) and (c) with Manabe scheme (contour interval .25 Pa/sec).

a.

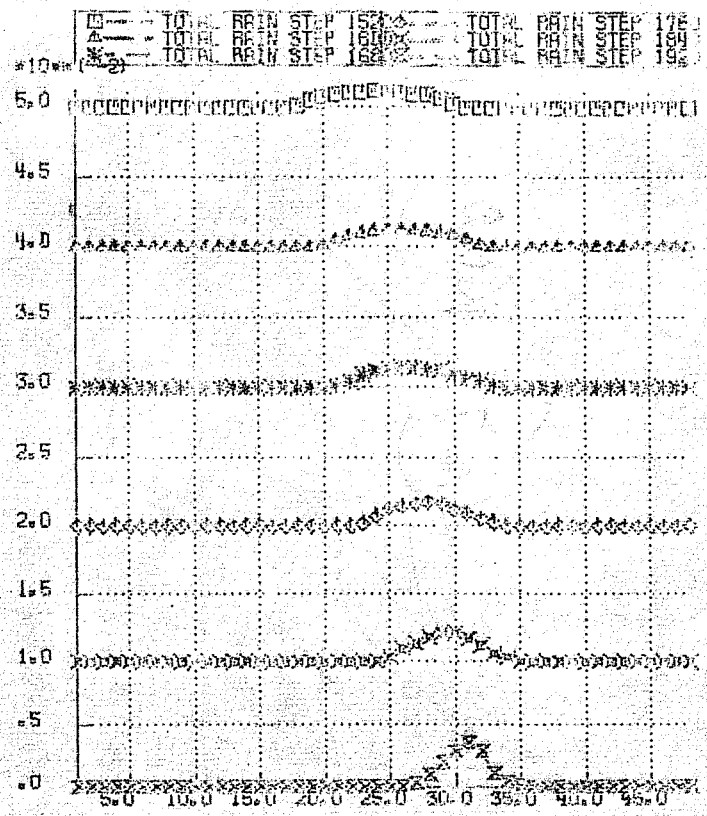

b.

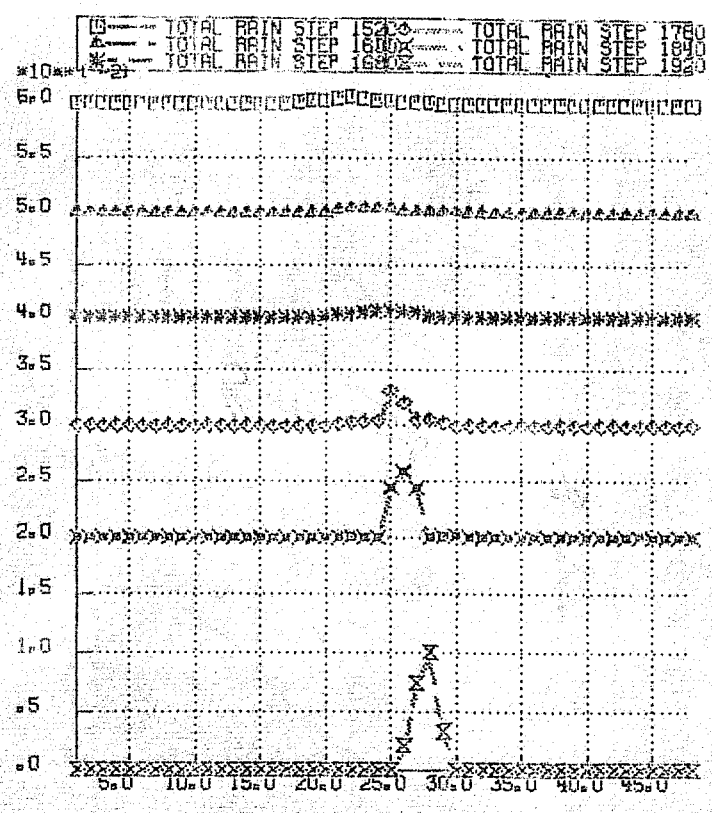

Fig. 15 Total accumulated precipitation in the periods day 0 h0 - day 1 h14 and the five 2-hour periods between d1 h14 and day 2 h0 at grid points in the runs illustrated in Figs. 11, 12 viz. (a) run with Kuo Scheme, (b) run with Manabe Scheme. The six periods are offset from zero for clarity. The top line represents the earliest period (day 0h0 - day 1 h14) while the bottom line represents the last period. The units are centimetres.

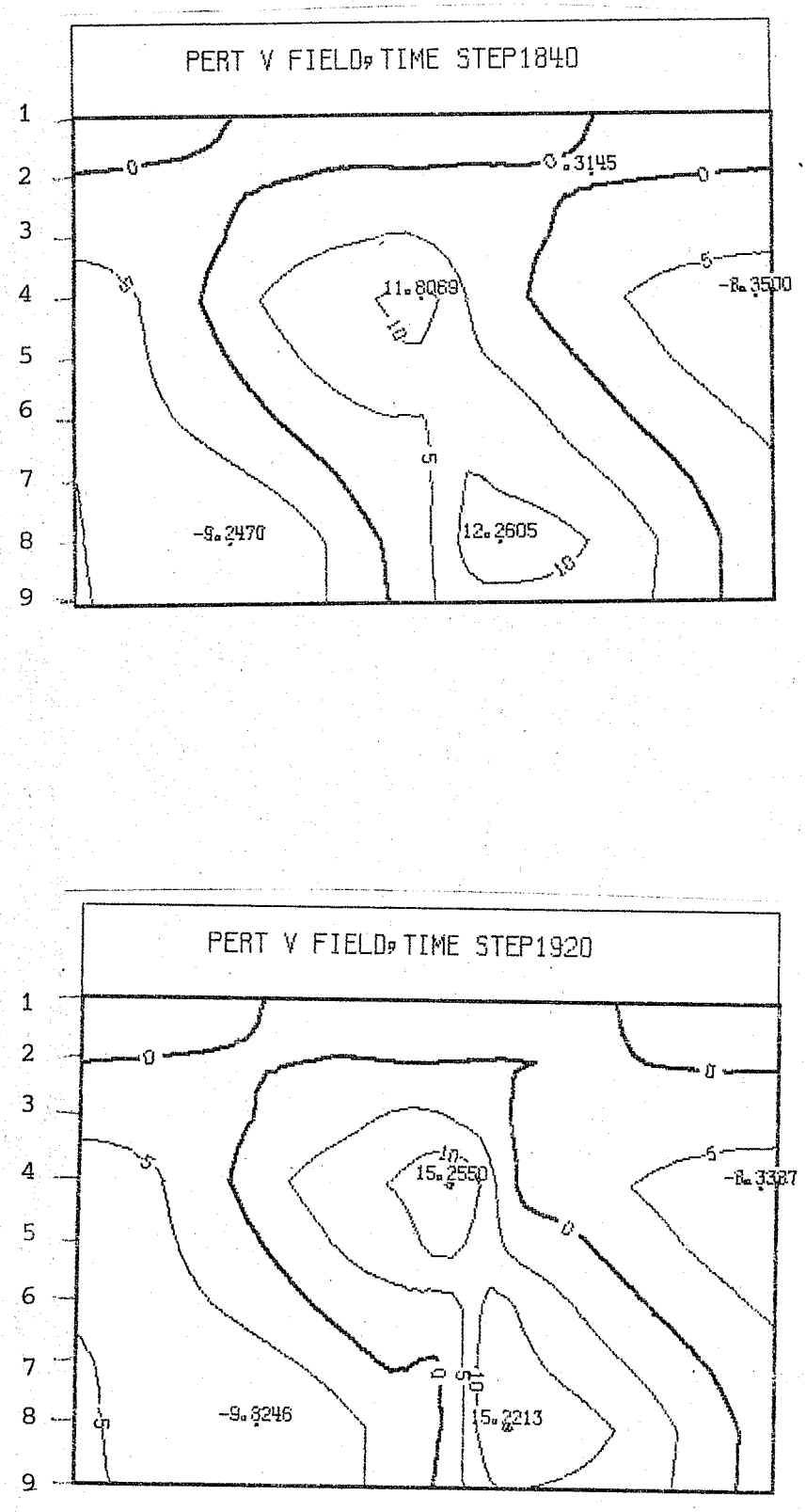

Fig. 16 The V' field at day 1 hour 22 and day 2 hour 0 in the run with the Manabe Scheme and a logarithmic specification for $\frac{\partial q}{\partial y}$.

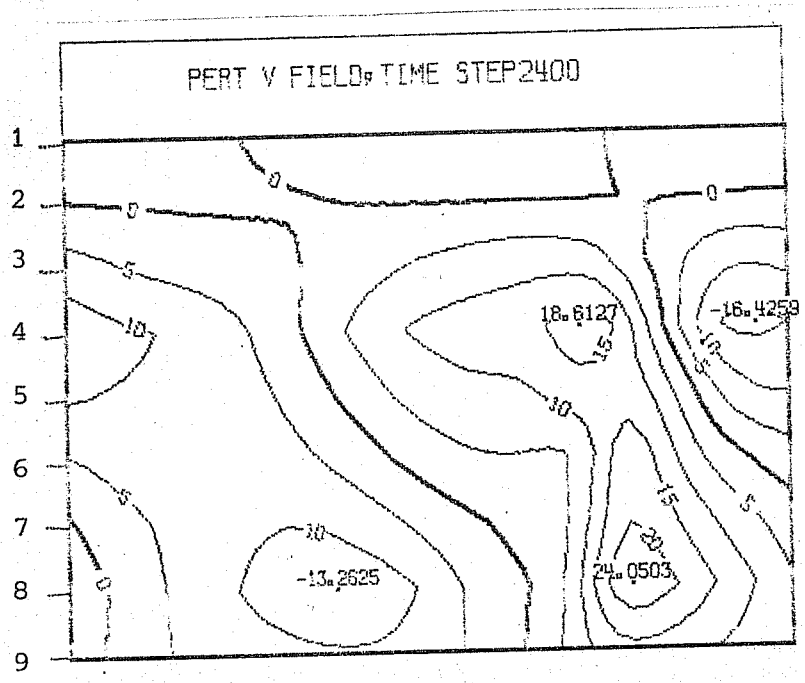

a.

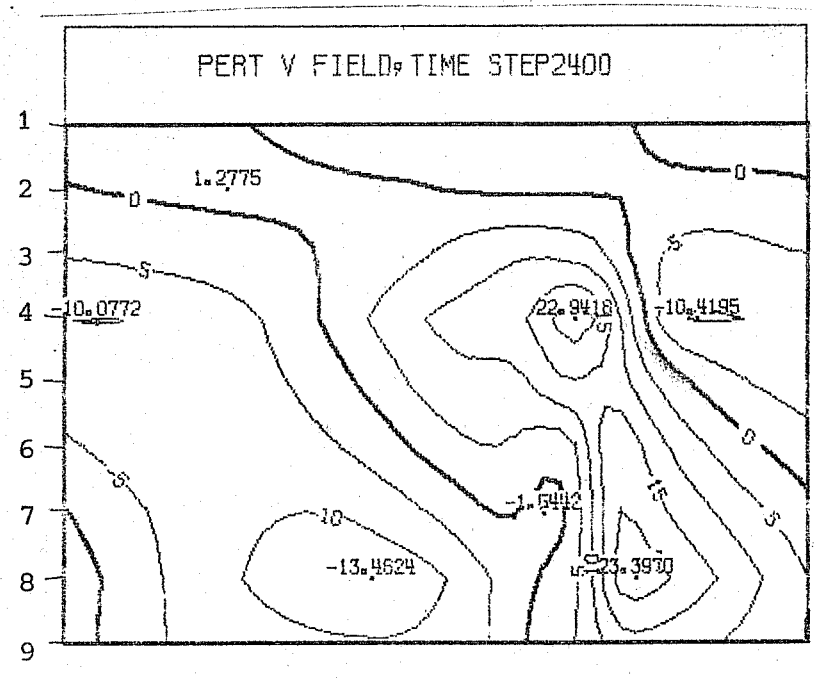

b.

Fig. 18 Field of V' at day 2 hour 12 in the runs with (a) the Kuo Scheme and (b) the Manabe Scheme where the specification for $\frac{\partial q}{\partial y}$ is linear.

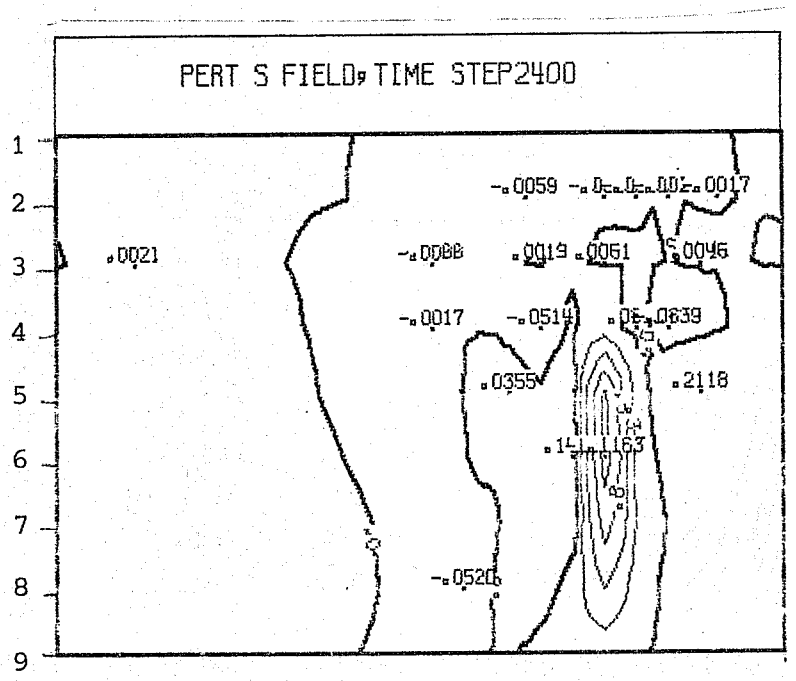

a.

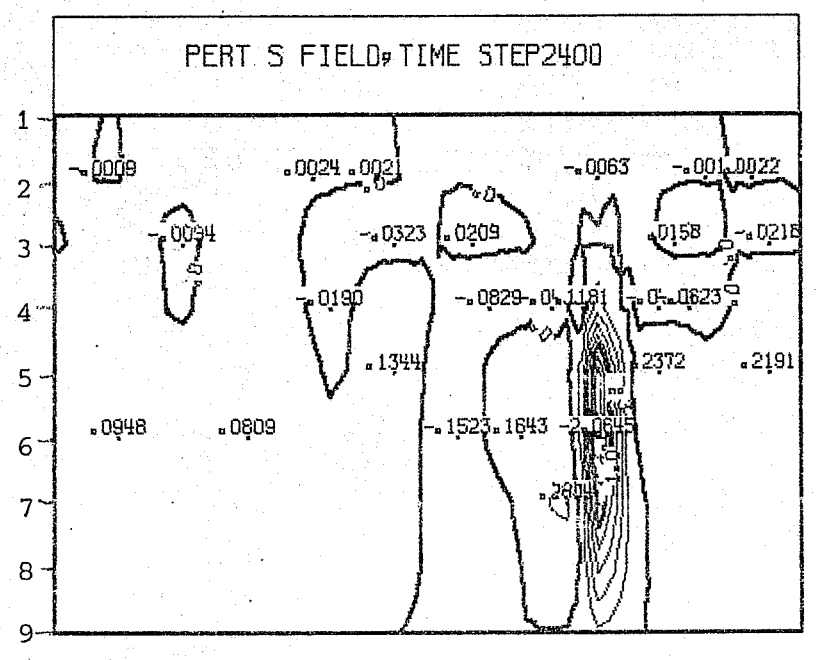

b.

Fig. 19 As Fig. 18 except for field of p*ω̇
Units are HPa/sec.

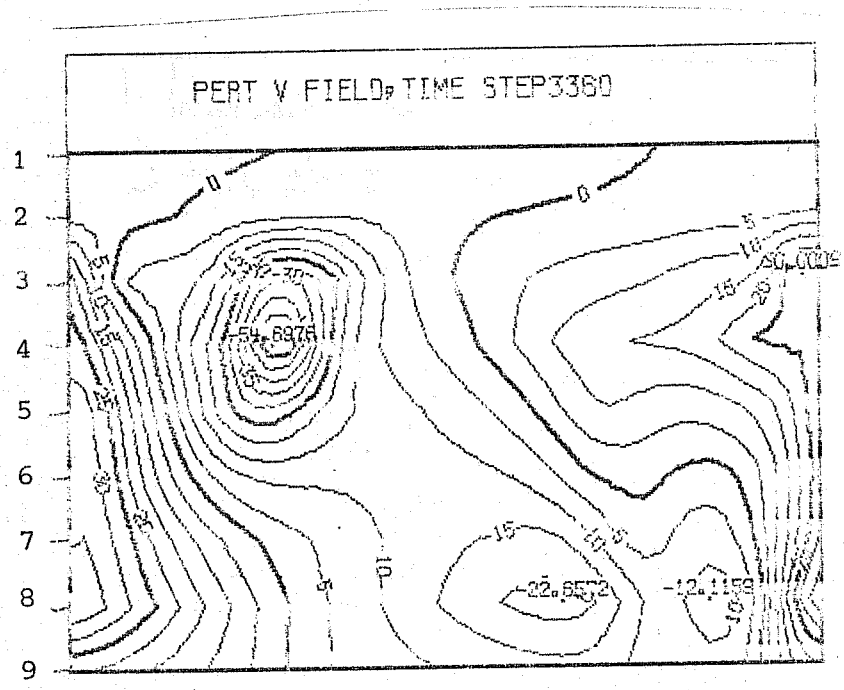

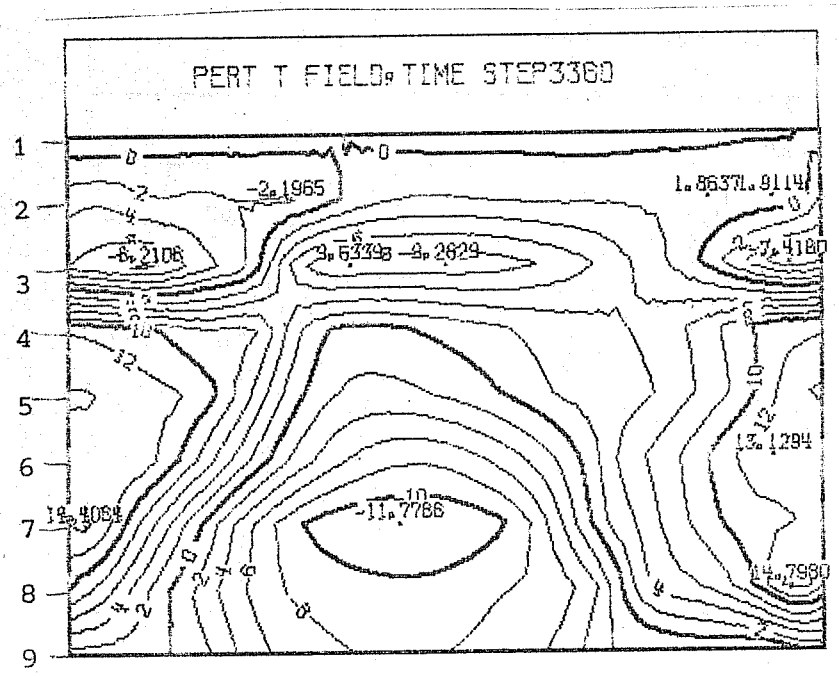

Fig. 20 Fields of V',T' at day 3½ for run with the Manabe Scheme and a linear specification $\frac{\partial q}{\partial y}$.

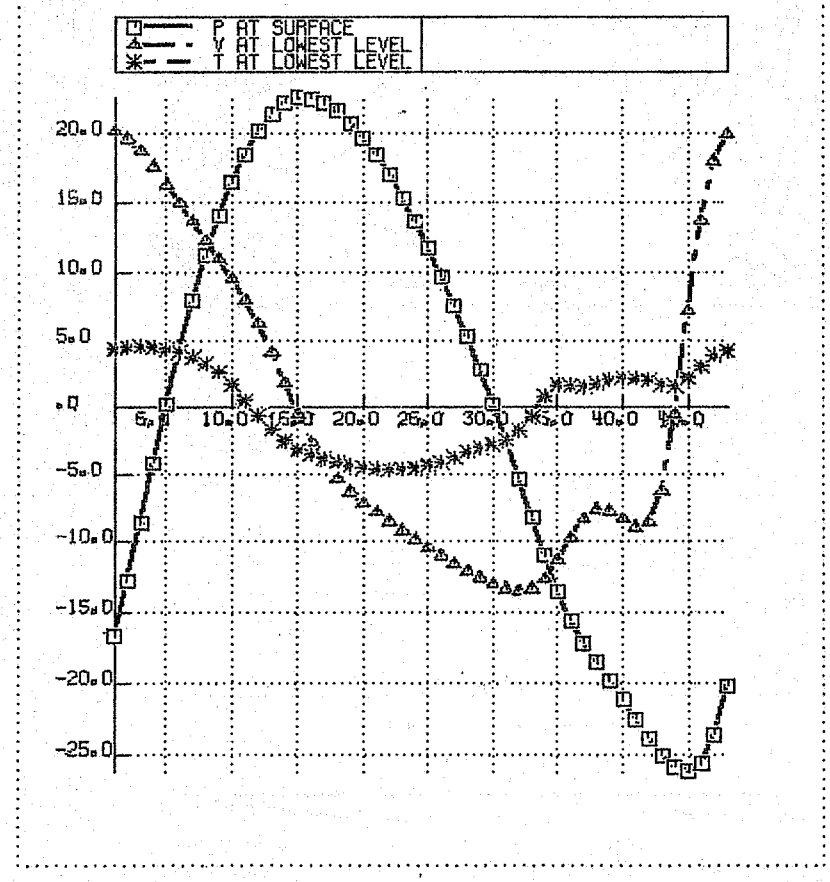

Fig. 21 Zonal profiles of p* (□), V_9 (Δ), T_9 (*) at day 3½ in the run with the Manabe Scheme and a linear specification for $\frac{\partial q}{\partial y}$. The units are HPa, m/sec., ^{o}K respectively.

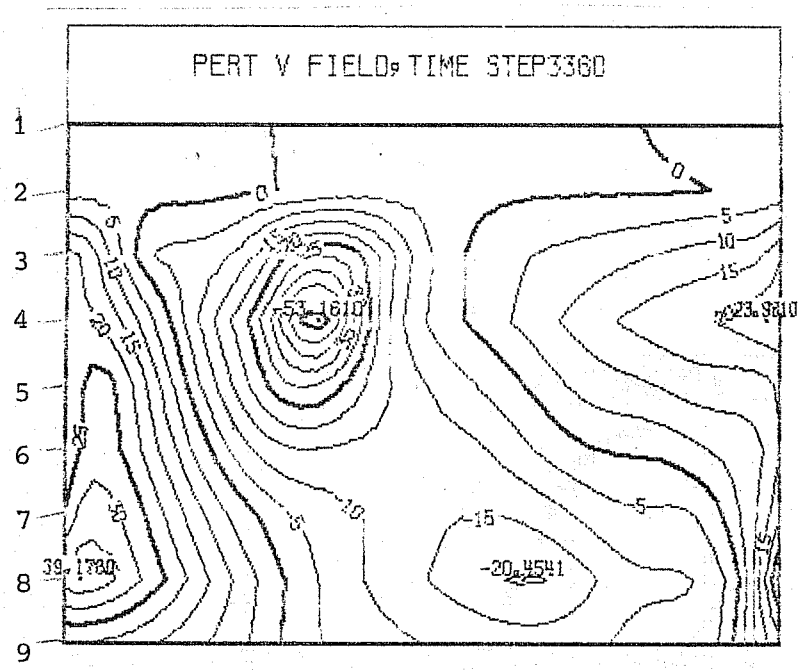

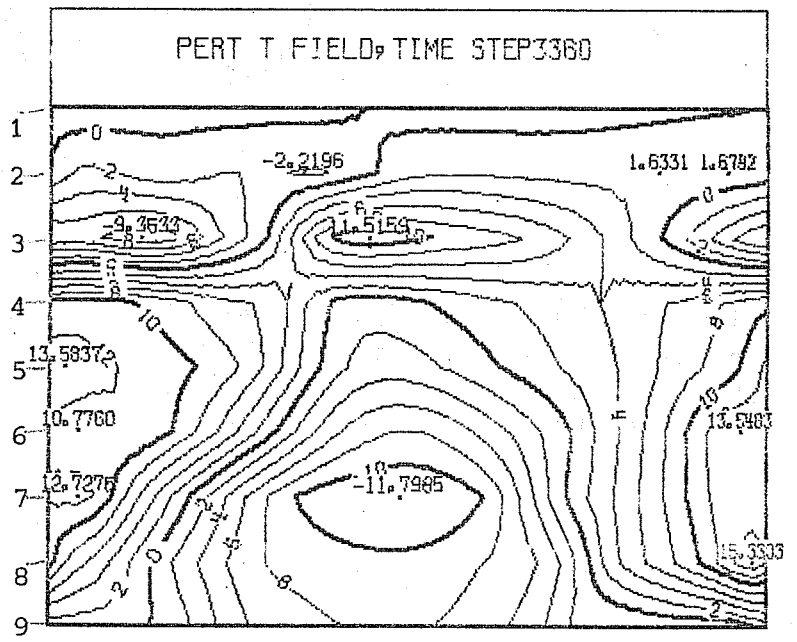

Fig. 22 The fields of V', T' at day 3½ in the run with the Kuo Scheme and a linear specification for $\frac{\partial q}{\partial y}$. The units are m/sec and °K.

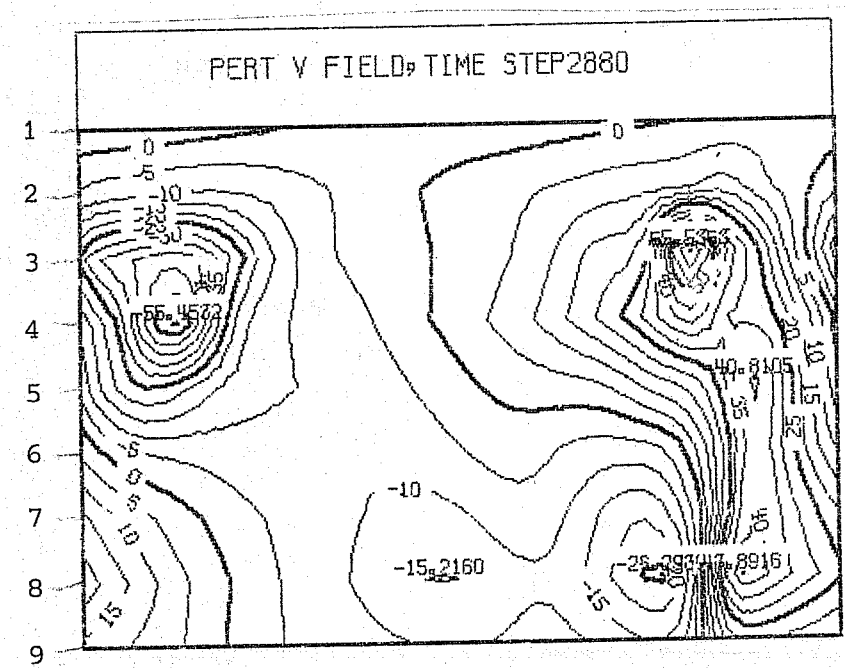

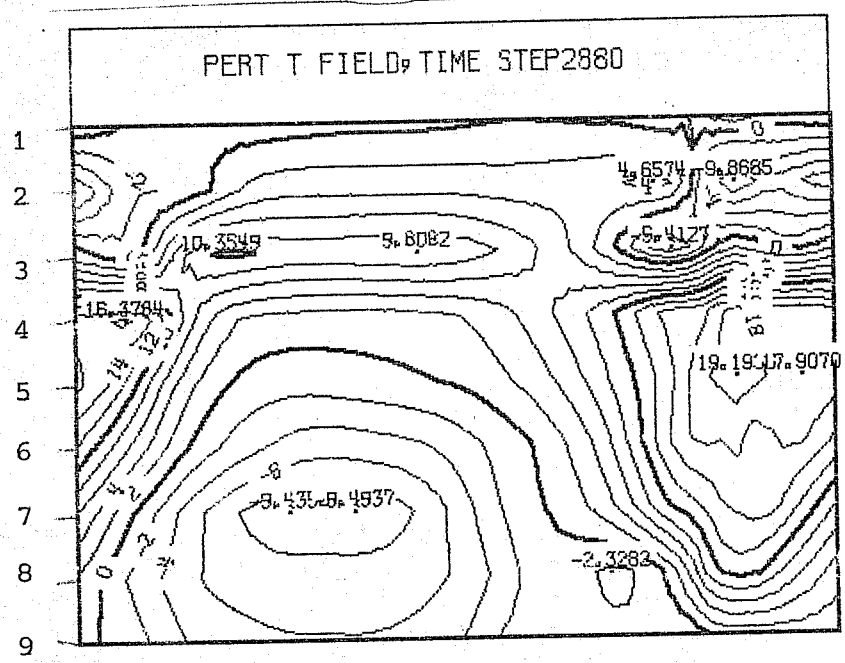

Fig. 23 The fields of V', T' at day 3½ in the run with the Manabe Scheme and logarithmic specification for $\frac{\partial q}{\partial y}$.

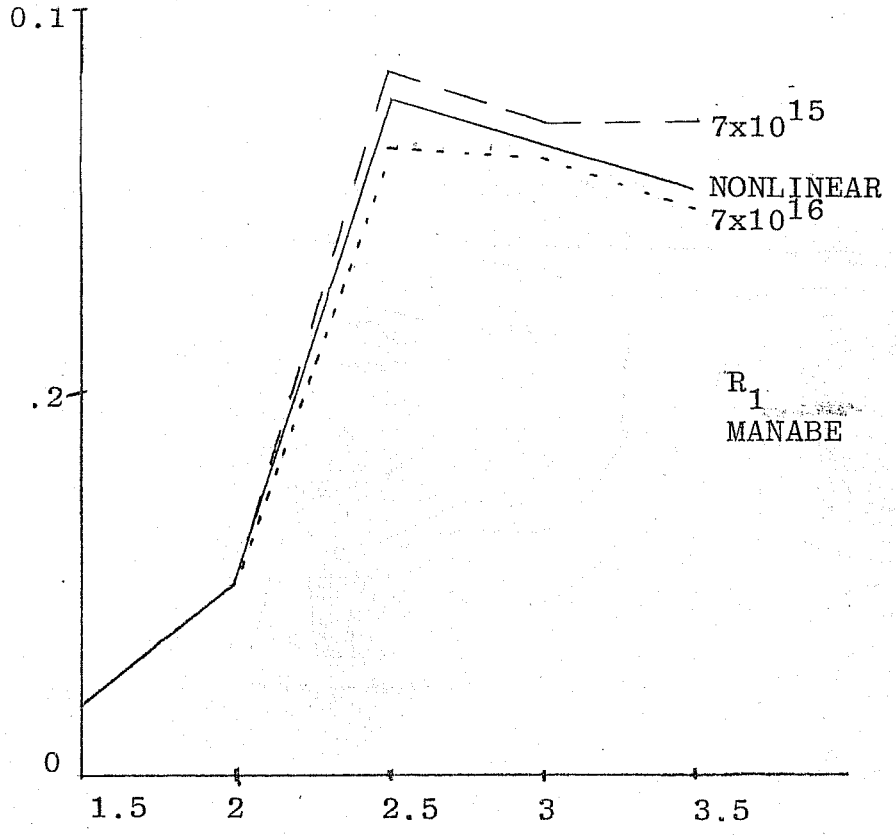

(a)

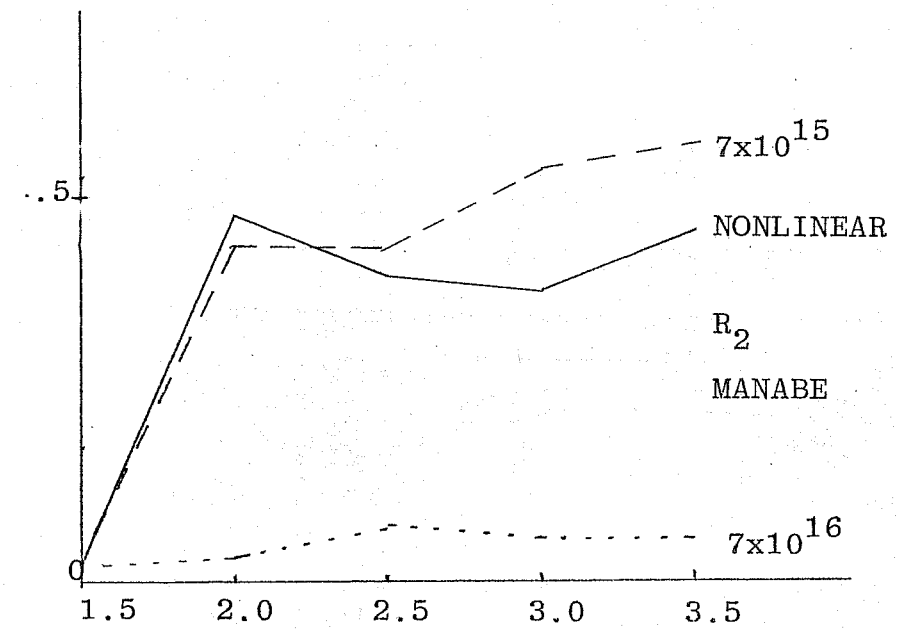

(b)

Fig. 24 (a) Time development of the ratio R_1 of the divergent kinetic energy in wave numbers (2-11) to the divergent kinetic energy in wave number (1) in three runs with the Manabe Scheme: (---) run with $K_4 = 7 \times 10^{15}$, (——) run with non linear diffusion, (...) run with $K_4 = 7 \times 10^{16}$.

(b) Time development of the ratio R_2 of the divergent kinetic energy in wave numbers (12-24) to the divergent kinetic energy in wave numbers (2.11) in the same three runs.

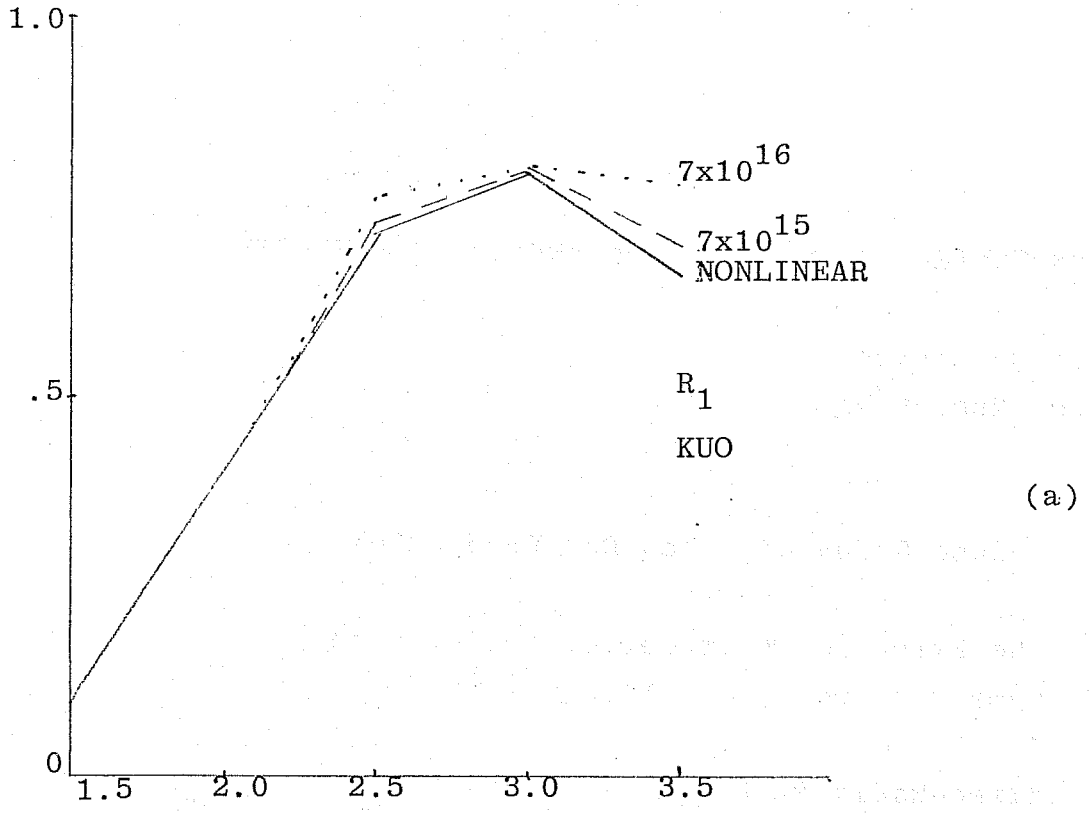

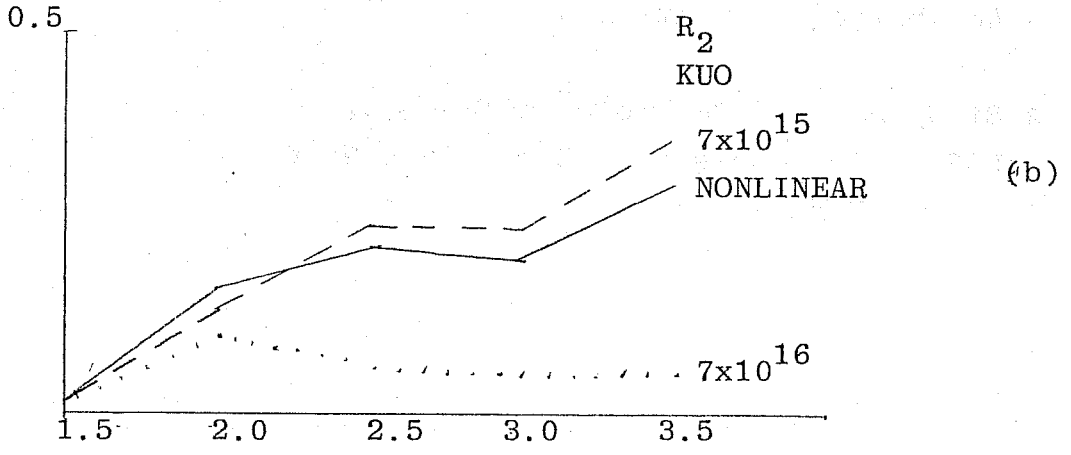

Fig. 25 As Fig. 3 except that the runs are done with the Kuo Scheme.

EUROPEAN CENTRE FOR MEDIUM RANGE WEATHER FORECASTS

Research Department (RD)
Technical Report No. 5

No. 1 A Case Study of a Ten Day Prediction

No. 2 The Effect of Arithmetic Precision on some Meteorological Integrations

No. 3 Mixed-Radix Fast Fourier Transforms without Reordering

No. 4 A Model for Medium Range Weather Forecasting - Adiabatic Formulation -

No. 5 A Study of some Parameterisations of Sub-Grid Processes in a Baroclinic Wave in a Two-Dimensional Model